12-2009

The Cryogenic Bonding Evaluation at the Metallic-Composite Interface of a Composite Overwrapped Pressure Vessel with Additional Impact Investigation

Eric A. Clark
Utah State University

THE CRYOGENIC BONDING EVALUATION AT THE METALLIC-COMPOSITE INTERFACE OF A COMPOSITE OVERWRAPPED PRESSURE VESSEL WITH ADDITIONAL IMPACT INVESTIGATION

by

Eric A. Clark

A thesis submitted in partial fulfillment
of the requirement for the degree

of

MASTER OF SCIENCE

in

Mechanical Engineering

Approved:

_____	_____
Dr. Thomas H. Fronk Major Professor	Dr. Steve L. Folkman Committee Member
_____	_____
Dr. Yibin Xue Committee Member	Dr. Byron R. Burnham Dean of Graduate Studies

UTAH STATE UNIVERSITY
Logan, Utah

2009

ABSTRACT

The Cryogenic Bonding Evaluation at the Metallic-Composite Interface of a Composite Overwrapped Pressure Vessel with Additional Impact Investigation

by

Eric A. Clark, Master of Science

Utah State University, 2009

Major Professor: Dr. Thomas H. Fronk
Department: Mechanical and Aerospace Engineering

A bonding evaluation that investigated the cryogenic tensile strength of several different adhesives / resins was performed. The test materials consisted of 606 aluminum test pieces adhered to a wet-wound graphite laminate in order to simulate the bond created at the liner-composite interface of an aluminum-lined composite overwrapped pressure vessel. It was found that for cryogenic applications, a flexible, low modulus resin system must be used. Additionally, the samples prepared with a thin layer of cured resin – or prebond – performed significantly better than those without. It was found that it is critical that the prebond surface must have sufficient surface roughness prior to the bonding application. Also, the aluminum test pieces that were prepared using a surface etchant slightly outperformed those that were prepared with a grit blast surface finish and performed significantly better than those that had been scored using sand paper to achieve the desired surface finish.

An additional impact investigation studied the post impact tensile strength of composite rings in a cryogenic environment. The composite rings were filament wound with several combinations of graphite and aramid fibers and were prepared with different resin systems. The rings were subjected to varying levels of Charpy impact damage and then pulled to failure in tension. It was found that the addition of elastic aramid fibers with the carbon fibers mitigates the overall impact damage and drastically improves the post-impact strength of the structure in a cryogenic environment.

(124 pages)

ACKNOWLEDGMENTS

I would like to sincerely thank Dr. Thomas Fronk for his all of his help and support throughout my time as a graduate student – especially all the time he spent helping me with my thesis. Without his guidance, direction, and help in answering my questions, this would not have been possible.

I would also like to thank HyPerComp Engineering Inc. and Michael Lambert for all of their help and support throughout the course of this project. Additionally, I would to express appreciation to committee members Drs. Steven Folkman and Yibin Xue for their support and assistance.

I would especially like to thank my family and friends for their encouragement and patience not only while I've been working on this document but also throughout my entire collegiate career.

Eric A. Clark

CONTENTS

LIST OF TABLES

LIST OF FIGURES

CHAPTER 1

INTRODUCTION

Section 1.1 – NASA Phase II STTR

In the spring of 2007, the National Aeronautics and Space Administration (NASA) awarded HyPerComp Engineering, Inc. (HEI) in conjunction with Utah State University (USU) a Phase II Small Business Technology Transfer (STTR) Contract. The work and research performed and that which is still being undertaken have been conducted in an effort to meet the benchmarks outlined by this contract.

Section 1.2 – HyPerComp Engineering, Inc.

HEI is a research and development firm located in Brigham City, UT that specializes in the design, fabrication, and testing of composite overwrapped pressure vessels (COPV's). Founded in 1996, HEI has become a world leader in designing COPV's for use in the alternative fuel, aerospace, and medical industries. They have been the recipient of several Phase I and Phase II NASA Contracts wherein they have received funding to research new materials and methods of fabrication for impact resistant, multi-use COPV's designed for deep space applications.

Section 1.3 – NASA Phase I Contract and Results

Due to their high strength to weight and stiffness to weight ratios, composite materials have developed into the primary candidates for many aerospace applications. One main area in which the benefits of composite materials would be paramount is use in

pressure vessels for storing liquid hydrogen and liquid oxygen for spacecraft propellant. Some estimate that the total pressure vessel weight could be reduced by as much as 35 percent if composite materials were to replace an all metallic vessel [1].

Prior to using these futuristic materials in real-world aerospace applications, their properties must be characterized in a deep space environment. The goal of the Phase I Contract was to investigate the behavior of various composite fibers and resins at cryogenic temperatures.

The data obtained from the Phase I Study demonstrates conclusively that any composite material utilized in COPVs in a cryogenic/impact environment must be designed and qualified with data from representative environments. Typically aerospace designs are extremely weight critical and historically tend to ignore the degradation due to cryogenic environments that was demonstrated during Phase I contract. Based on the data collected during the Phase I STTR, it can be stated conclusively that the failure to recognize the degradation of mechanical properties at cryogenic temperature will almost certainly lead to reduced margins of safety if not worse consequences.

Section 1.3.1 – Cryogenic Impact Testing on Neat Resin Systems

Several resin systems were selected for ambient and cryogenic impact testing. The resin systems included typical “wet” winding systems and a typical “prepreg” winding system. The test consisted of cutting the specimens to 0.39 in wide by 0.39 in thick by 2.5 in long. Izod impact tests were performed and the energy required to fracture the specimen was recorded, providing a quantitative measurement of the impact strength. All neat resin systems were tested at ambient temperature as well as liquid

nitrogen (LN_2) temperature (at ambient pressure, the boiling temperature for LN_2 is -314°F).

Figure 1 below illustrates the results of the impact testing for several different resin systems including commercial resins from Epon, a prepreg system from ATK/Thiokol TCR, and several experimental resins including HEI 535 from HyPerComp Engineering.

Section 1.3.2 – Cryogenic Impact and Tensile Testing

From the neat resin cryogenic impact testing, two resin systems were selected for inclusion into a composite cryogenic impact testing evaluation. The first resin system selected was HEI 535, due to its outstanding performance in the neat resin impact tests.

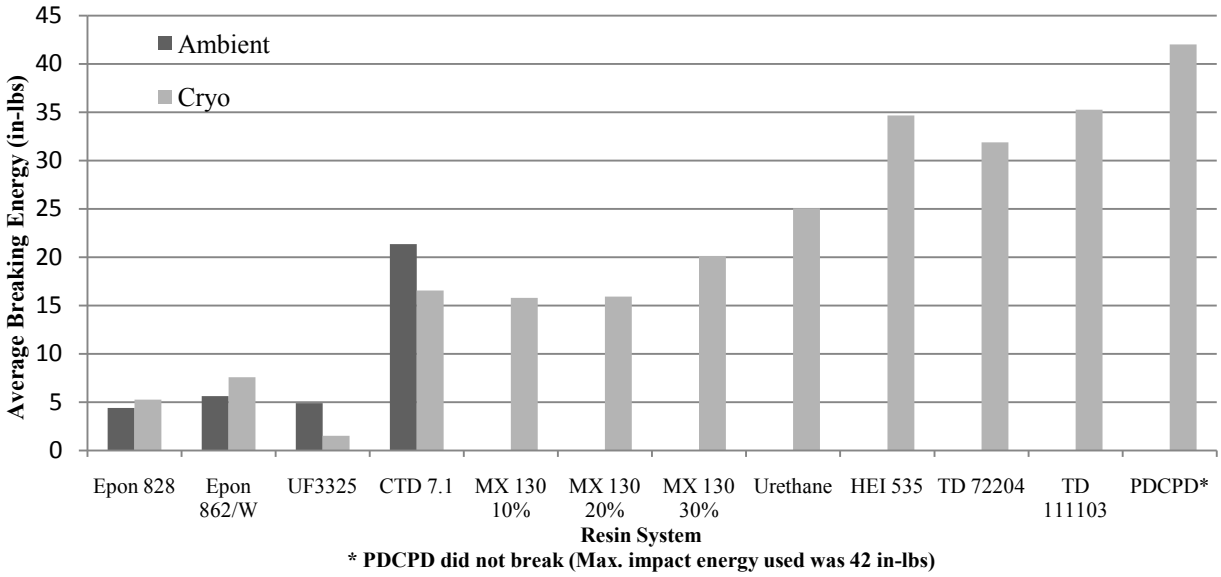

Figure 1. Ambient and cryogenic Izod impact test results.

The second resin system selected was Epon 828. This resin system a widely used resin system for composite materials and thus provides a baseline for comparison.

The selection of the fiber material was based on previous impact related NASA SBIR projects performed by HEI (Contracts NAS8-01146 and NAS8-02101) and availability of the material. Zylon fiber was used based on its excellent robustness properties. The team also decided on the use of Hexcel's IM7 carbon fiber due to its availability and excellent cryogenic performance in a previous NASA SBIR project (Contract NNM04AB16C).

These selections made for six different composite material layups. Table 1 summarizes these material layups.

Flat panel composite coupons with a layup of $[0_2/90_3/0_2]$ were first impacted and then subsequently pulled in tension. The cross ply layers (90°) were inserted to prevent the tensile failure of the resin (transverse to the fiber) during tensile testing. These layers were all made of the same material for each specimen and they did not contribute to the tensile structural ability of the specimen. The overall thickness of the specimen was approximately 0.040 in. This of course varied slightly from specimen to specimen depending on which material was used (i.e. IM7 or zylon).

Table 1. Summary of Composite Layups for Cryogenic Testing

Fiber Material	Resin System
IM7	Epon 828
IM7	HEI 535
Zylon	Epon 828
Zylon	HEI 535
IM7 / Zylon	Epon 828
IM7 / Zylon	HEI 535

After performing tests at ambient conditions in order to identify a baseline capability, subsequent coupon specimens were subjected to a Charpy impact, by a target

energy level while at LN_2 temperature. Two separate energy levels were selected to provide the following effect. After the specimen had been impacted at LN_2 temperature, it was then subsequently tensile tested at LN_2 temperature.

In order to evaluate the results, a Finite Element analysis was performed. The average failure load per unit width (lb/in) was used to determine the delivered fiber strength of the composite. The delivered fiber strength is the resultant ultimate tensile strength of the fiber itself (not the composite). Figure 2 shows the delivered fiber strength for each fiber/resin system. All IM7 fiber systems show significant degradation from a cryogenic impact. All zylon fiber systems show excellent promise as a cryo-impact resistant material system, while the best performance was demonstrated by the HEI 535 resin system. The IM7/zylon hybrid systems also show degradation from cryogenic impact.

The aforementioned Phase II Contract was awarded at the conclusion of the Phase I collaboration between HEI and USU.

Table 2. Impact Energy Levels

Energy Level	Value (in-lb)	Desired Effect
Low	12.5	Minimal visual effect, fibers do not show damage
High	20.5	Visual effect, fibers may show damage

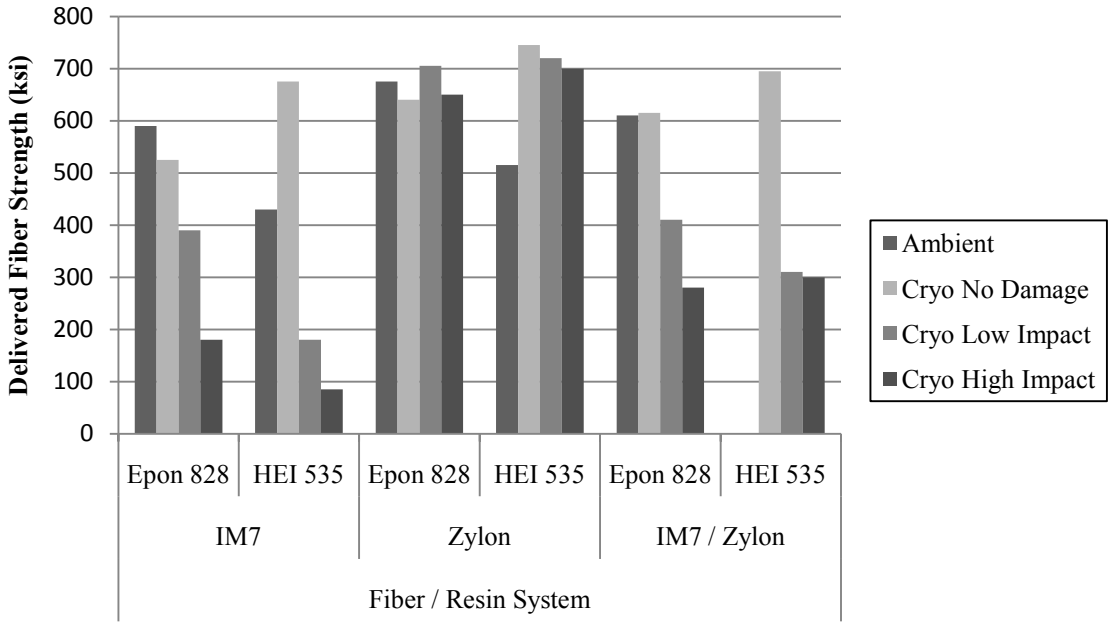

Figure 2. Delivered fiber strength for each of the fiber/resin systems tested.

Section 1.4 – Proposed Work of the NASA Phase II Contract

The Phase II Proposal, written by Jared Noorda – HEI design engineer – and Dr. Thomas Fronk – mechanical and aerospace engineering associate professor – focuses on recapitulating what was learned during the course of the Phase I contract, then conducting more comprehensive research in the same areas of interest, specifically the impact properties of composite samples at cryogenic temperatures. Additionally, a significant portion of the contract was devoted to investigating the tensile properties of various resin systems at cryogenic temperatures.

CHAPTER 2

LITERATURE RESEARCH

An extensive literature review was conducted at the beginning of the contract, specifically examining any prior research publications conducted in the following areas:

- Impact
  - Impact Testing of Composite Materials
  - Impact Properties of Neat Resin Systems
  - Composite Fibers and Impact Resistance
  - Temperature Effect on Impact Properties
  - Impact Resistant Materials

- Fracture Properties of Composites
  - Composite Fracture Properties
  - Adhesive Fracture
  - Temperature Effect on Fracture Properties
  - Fracture Behavior of Composite Materials

- Bonding
  - Bondline Thickness
  - Bonding Dissimilar Materials
  - Adhesive Properties
  - Cryogenic Bonding
  - Surface Treatment

A brief summary of the key research papers are given in the following sections.

Section 2.1 – Impact

Due to the many advantages of composite materials, extensive research is being conducted to better understand the behavior of composite structures under impact loading at cryogenic temperatures. Gomez-del Rio et al. studied the effect of low velocity impact by means of a drop weight tower, on square composite coupons at cryogenic

temperatures. They found that cooling the composite before the impact has an effect similar to that of increasing the impact energy [2].

K. Ohtani et al. evaluated the material response of fiber-reinforced composite plates at cryogenic temperatures due to hypervelocity impact, which results in perforation due to the inertial effects of the projectile [3]. Similarly, Lopez-Puente et al. have studied the effect of medium and high speed velocity impacts on square composite coupons using a tempered steel projectile. They found that cryogenic temperatures had a negative effect on the impact resistance of the composites when they were subjected to a medium velocity impact. Their results also showed a damage saturation effect once the projectile reached ballistic velocity. At that velocity, temperature had no effect on the damage sustained by the composite [4].

Whitley and Gates have studied the tensile and stiffness properties of different composite materials subjected to a cryogenic environment. They found that as the materials approached -200° C (-328° F) their strengths decreased. However, if the temperature was lowered past -200° C the strength would be lower than at room temperature, but higher than the strength at -200° C [5].

Regarding hybrid fiber-reinforced composites to improve impact resistance, work done by Saka and Harding (1990) demonstrated in an ambient environment that hybridizing an all carbon laminate with a more elastic glass fiber significantly increased the failure strain above the mean value of the all carbon laminate alone [6].

Section 2.2 – Fracture Properties

The introduction of a lower strength (high elastic or high energy absorbing) fiber into a composite structure has been shown to have advantageous results, requiring more impact energy for crack propagation [7].

R.J. Melcher et al. studied the Mode I fracture toughness of an adhesively bonded composite-composite joint in a cryogenic environment. Their results show that at room temperature stable crack propagation was observed, however at cryogenic temperatures, they documented a slip-stick fracture mode of failure where the crack would suddenly propagate then subside in a repetitive pattern. They also observed a substantial decrease in the fracture toughness at cryogenic temperature compared to room temperature [8].

Section 2.3 – Bonding

Section 2.3.1 – Surface Preparation

Goeders and Perry of McDonnell Douglas Space Systems investigated adhesive bonding at cryogenic temperatures. As part of this study, six surface preparations were examined. The samples subjected to an aluminum oxide grit blast preparation resulted in the highest shear strength [9]. Also, G. Lawcock et al. showed that the use of surface etchants on aluminum adherents resulted in a higher bond strength and prevented failure at the aluminum interface [10].

Section 2.3.2 – Resin Additives

Xiaolong Hu and Pengcheng Huang conducted research which measured the peel strength, lap shear strength, and fracture strength at cryogenic temperatures. They

concluded that the addition of a polyether toughener to an epoxy adhesive improved the bond-strength properties against shear and tension [11].

Section 2.3.3 – Bondline Thickness

T. Shimoda et al. performed extensive testing of double-lap tensile specimens of Carbon Fiber Reinforced Polymer (CFRP) and Aluminum adherents with different bond thicknesses. These tests were also performed over a wide range of temperatures. Based on their results, they concluded that the bond strength is very sensitive to bond thickness and uneven bond application [12].

CHAPTER 3

BONDING INVESTIGATION

One of the main uncertainties this contract set out to clarify is the structural integrity of a thin-walled, aluminum lined COPV. In the struggle to conserve weight for deep space applications, it is highly desired for these vessels to be as light as possible. One way to reduce weight is to chemically etch the sidewall of the aluminum liner, reducing its thickness. This however raises a concern that when the vessel is depressurized, the resulting compressive stress associated with the elastic recovery of the composite overwrap will cause the thin-walled liner to buckle. Hence, the need for a superior bond that can maintain its integrity at cryogenic temperatures between the composite and the liner is vital.

Additionally, NASA Engineer David E. Glass stated that there are numerous cryogenic tank designs for reusable launch vehicles. Many of the designs for storing the propellant require cryogenic insulation that will need to be bonded to the outside of the tank [13].

Section 3.1 – Variables to Be Investigated

Based on the results from the Phase I study as well as the literature research, it was determined that a comprehensive understanding of the following variables is crucial to the success of achieving an acceptable bond at the composite-aluminum interface:

- Resins / Adhesives
- Surface Preparation
- Temperature Effects
- Bondline Thickness

Section 3.1.1 – Resins / Adhesive

Based on the literature review several commercial as well as experimental resin systems were included in the investigation, including both epoxy and urethane resins. The experimental resin systems have been specifically formulated for low temperature environments. Additionally, resin systems that performed well in the Phase I study were also included in the test population.

Section 3.1.2 – Surface Preparation

As discovered during the review of the Goeders and Perry publication based on the McDonnell Douglas Space Systems bonding investigation, changing the condition of the bonding surface can have dramatic results on the strength of the bond. Several different surface preparation techniques were examined including various abrasion techniques as well as a the use of a surface etchant.

Section 3.1.3 – Temperature Effects

As these tests were being conducted to characterize materials for use in a deep space environment, it was important to understand their behavior at extreme temperatures. The tests were performed at both ambient conditions as well as when the test samples were submerged in LN_2, such that a measure of the degradation due to the cryogenic environment could be obtained.

Section 3.1.4 – Bondline Thickness

In the text, *Fracture Mechanics*, author T.L. Anderson uses a fracture based analysis to conclude that in general, a sample with a thin bondline will have a higher

fracture toughness (K_{IC}) than an identical sample with a thick bondline. This is due in part that for a sample with a thin bondline, adhesive necking will be constrained while the adhesive in a thick bondline will be free to neck. For a more in depth discussion on this analysis, see [14]. Based on Anderson's explanation it was determined that a thin bondline would perform the best; however several bondline thicknesses were included in the investigation to find the optimum thickness.

CHAPTER 4

TESTING

Table 3 outlines the various tests that were performed as well as the parameters investigated and the properties tested. A representative test matrix for each of the tests outlined in the table below is given in Appendix A.

Table 3. Testing Description

Test	Parameters	Properties
Double Lap Shear Tests (ASTM D3528-96)	Surface Preparation	Adhesive Shear Strength
	Bondline Thickness and Resin Systems	
	Cryogenic Temperature Effects	
Tensile Tests (ASTM D952-02)	Surface Preparation	Adhesive Tensile Strength
	Bondline Thickness and Resin Systems	
	Cryogenic Temperature Effects	
Buckling Tests	Surface Preparation	Adhesive Tensile Strength
	Bondline Thickness and Resin Systems	Buckling of Thin Aluminum Liner
	Cryogenic Temperature Effects	
Impact Tests (ASTM D2290-04)	Fiber Combinations and Resin Systems	Charpy Impact Breaking Energy
	Impact Energy	Post Impact Tensile Strength
	Cryogenic Temperature Effects	

ASTM Test Standards for the shear, tensile and impact tests were obtained and followed as a guideline; however deviations were made in order to allow the samples to be tested in a cryogenic environment. A more detailed description of the testing procedures is given in subsequent sections.

Section 4.1 – Double Lap Shear Test

An important test to gain qualitative information regarding the previously mentioned variables is the double-lap shear test. These tests were intended to help identify how different resin systems performed when subjected to a state of shear. Additionally, by performing the tests at both ambient and cryogenic conditions, an understanding of the reduction in shear strength due to the thermal stress could be obtained.

The test procedure outlined in ASTM D3528-96, Standard Test Method for Strength Properties of Double Lap Shear Adhesive Joints by Tension Loading, was used as a guideline for the sample preparation and test procedure [15]. This test method is designed to produce shear property data for the process control and specification of adhesives

Section 6.0 of the standard outlines two acceptable test sample configurations. For the testing being described, a Type B specimen was used as illustrated in Figure 3.

Section 4.1.1 Test Sample Preparation

The double-lap shear specimens fabricated by HEI test engineers consisted of two aluminum pieces bonded to two composite graphite laminates. A representative test

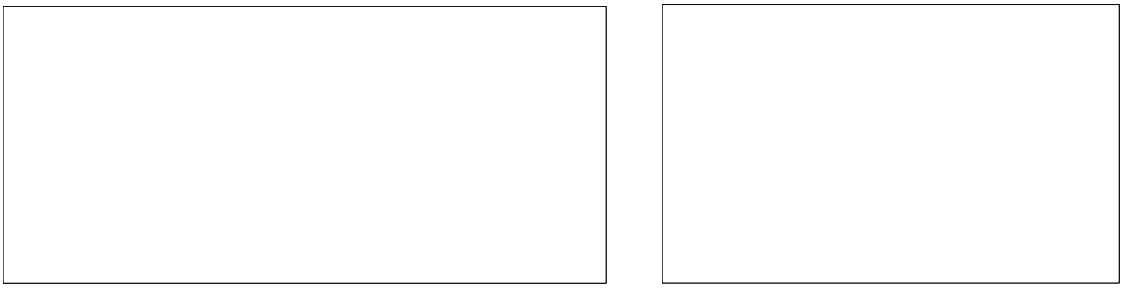

Figure 3. A Type B, Double Lap Shear test sample.

matrix can be found in Table A-1 of Appendix A. The variables investigated are discussed in the sections below.

Section 4.1.1.1 – Resin Systems

Two resin systems were chosen to be included in the double lap shear test matrix, HEI 535 as well as an experimental urethane resin system. HEI 535 is a resin system formulated by HEI design engineers for cryogenic applications. It is an intermediate modulus epoxy resin that partially retains its flexibility even at low temperatures. This resin system was tested extensively during the Phase I contract and performed well when subjected to extreme temperatures.

The urethane resin system selected is an experimental resin system formulated by NASA MSFC.

Section 4.1.1.2 – Surface Preparation

Prior to bonding, the bond area of half of the aluminum samples were scored with course 100 grit sandpaper, while the remaining specimens were lightly abraded with 180 grit sandpaper.

Section 4.1.1.3 – Bondline Thickness

Two different bondline thicknesses were evaluated; a thin bondline of 0.005 in as well as a thick bondline measuring 0.015 in were used. The bondline thickness was controlled using metallic shims.

Section 4.1.1.4 – Double Lap Shear Test Procedure

The test parameters specified in the ASTM Standard were followed as closely as possible. However, as the tests were performed at both ambient conditions and at cryogenic conditions (submerged in LN_2), some modifications to the directives of the standard had to be made. The cryogenic specimens were wrapped in breather cloth and submerged in a LN_2 bath for one hour prior to testing. Thermocouples were attached to the bond to monitor the temperature throughout the test. Care was taken when loading the test samples not to subject the specimens to any type of torque or other force. All of the tests were performed with the Tinius Olson 10,000 lb Tensile Test Machine seen in Figure 4.

Section 4.2 – Tensile Tests

While the shear tests provided a lot of practical information and were helpful in identifying trends associated with certain adhesives and preparation techniques, it was determined at this point to transition from shear to tensile testing. As previously mentioned, the aim of these tests was to develop a strong bond between the composite overwrap and metallic liner of a COPV. If buckling were to occur during depressurization, there would be an associated Mode I tensile failure as the composite overwrap separated from the liner. As such, it was important to gain a thorough

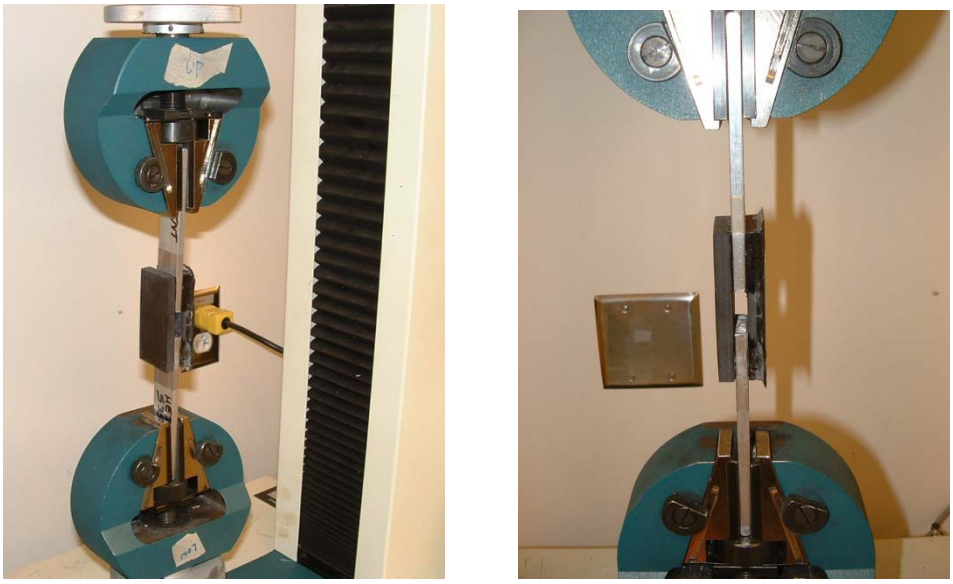

Figure 4. A Double Lap Shear test sample loaded in the Tinius Olson tensile testing machine.

knowledge of the tensile properties of the candidate materials. This was the main consideration in discontinuing the shear testing and to begin performing tensile tests. ASTM D952-02, Standard Test Method for Bond or Cohesive Strength of Sheet Plastics and Electrical Insulating Materials, was used as a guideline in conducting the tensile tests [16]. This standard outlines the testing for determining the bond strength or ply adhesion strength of both laminated and non-laminated thermoplastic and thermosetting materials. As with the shear tests, a minimal number of deviations were made from the standard. To lower the machining cost, circular test samples were used as seen in Figure **5**, as opposed to the square blocks designated in the standard. Additionally, modifications were made to the test fixture in order to allow the samples to be tested in a cryogenic environment.

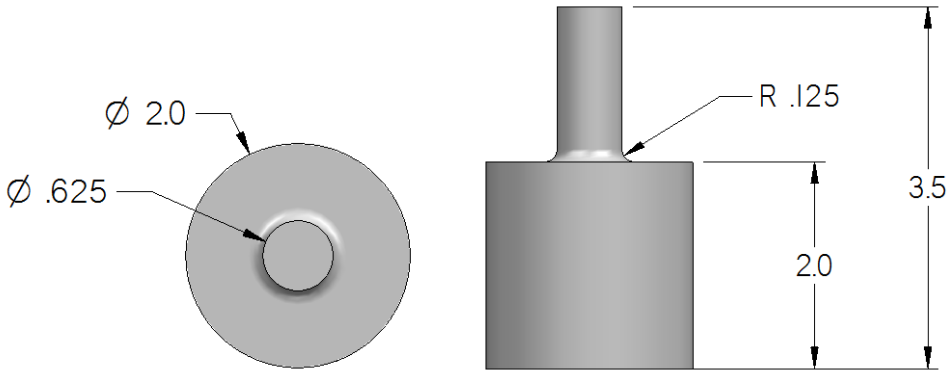

Figure 5. Aluminum test pieces used in the tensile testing.

Section 4.2.1 – Test Sample Preparation

The entire adhesive assembly is seen in Figure 6. The same parameters that were used in the Double Lap Shear tests were investigated for the tensile testing, namely surface preparation, temperature, bondline thickness, and the adhesives investigated. However, some changes were made within these parameters, based on the results of the shear tests. A detailed review of the variables is listed in the subsequent sections and a representative test matrix is outlined in Table A-2 of Appendix A.

Section 4.2.1.1 – Resin Systems

The two resin systems used in the double lap shear tests (HEI 535, urethane) were included in the tensile test population as well as two commercial resin systems.

The two additional resin systems included were West 105 and Epon 862. Both are typical commercial epoxy resin systems. Dr. Thomas Fronk had previously used the West 105 resin system on a limited basis and thought it would be informative to perform

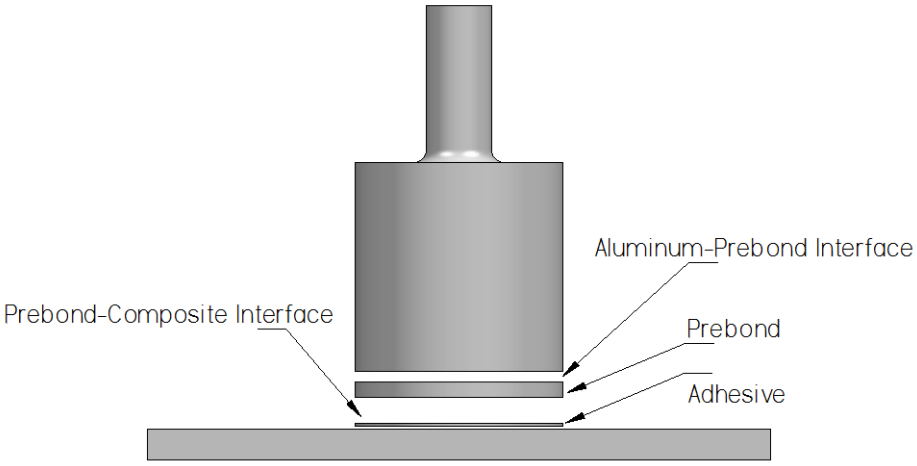

Figure 6. The aluminum test piece, prebond, adhesive and the composite laminate.

an in-depth evaluation of it. Epon 862 is a very common commercial resin system that is widely used in composite applications.

It is important to note that both of these resin systems are designed for use in ambient conditions; however they were included to see how they would behave when subjected to a low temperature environment.

Section 4.2.1.2 – Surface Preparation

After examining the results of the double lap shear tests, there was no discernable difference in the results between the samples that had been scored with 100 grit sandpaper and 180 grit sandpaper. Therefore, it was determined to first evaluate samples with an as machined surface compared with samples that had been scored by 100 grit sandpaper. The bond area of the as machined samples had a very smooth finish achieved from being turned on a lathe during the machining process. The surface finish of the sanded test samples was achieved by fixing a piece of 100 grit Aluminum Oxide

sandpaper to a flat surface and then placing the aluminum test pieces on the sandpaper and moving them in a circular pattern while applying a moderate amount of downward force. The sheet of sandpaper was changed frequently to ensure that each of the samples was subjected to the same amount of abrasion.

After several iterations, it was determined to experiment with the more aggressive techniques of grit blasting and the use of a surface etchant.

The grit blast samples were prepared using alumina grit and were prepared by a HEI test technician with extensive grit blasting experience.

The surface etchant chosen was AC 130 manufactured by Advanced Chemistry Technology (AC Tech). This product was recommended by NASA MSFC and is a high performance surface preparation designed to promote enhanced adhesion for bonding of aluminum alloys. The manufactures recommended application procedure was followed.

Regardless of the surface method employed, care was taken to make sure that the samples were prepared in a manner to avoid contamination. Also, the samples were prepared immediately prior to the actual bonding application in order to avoid any oxidation build up on the aluminum samples.

Section 4.2.1.3 - Prebond

The tensile tests were initially conducted by bonding the aluminum test pieces to already cured composite laminates. However, in an effort to more completely mimic the actual situation of an aluminum lined pressure vessel with a composite overwrap, the majority of the tensile tests were performed by applying the aluminum test pieces to an wet composite laminate and then the aluminum test fixtures and laminate were co-cured

together. One drawback of this manufacturing technique was that it became very difficult to control the bondline thickness.

As a solution to this obstacle, it was conceived to apply a thin layer of resin to the aluminum test piece and cure it following the aluminum surface preparation. This prebond enabled the bondline thickness to be controlled, and also acted as a shear-ply.

Both thick (0.015 in) and thin (0.005 in) prebonds were investigated using each of the different resins. Following the surface preparation of the aluminum test pieces, the prebonds were fabricated by adhering small metal shims of the desired thickness to the bottom of the aluminum test pieces. They were then placed in a Teflon coated resin bath and allowed to cure at ambient conditions until the resin had hardened. They were then cured at elevated temperatures using the manufacturers recommended cure profile. A band saw was used to trim off the excess resin from around the sides. The prebond was then measured and sanded down to the correct thickness as needed. Figure 7 illustrates a failed tensile test sample. Upon close examination, part of the prebond can be seen on the face of the aluminum test piece.

Section 4.2.2 – Tensile Bonding Procedure

Once the surface and prebond preparations were complete, it was time for the bonding process to the composite laminate. As previously mentioned, the initial tests were performed by adhering the aluminum test piece to an already cured composite laminate. However, the majority of the test pieces were applied to a wet wound composite laminate and co-cured together.

This process consisted of filament winding a flat mandrel with TR 50-S graphite

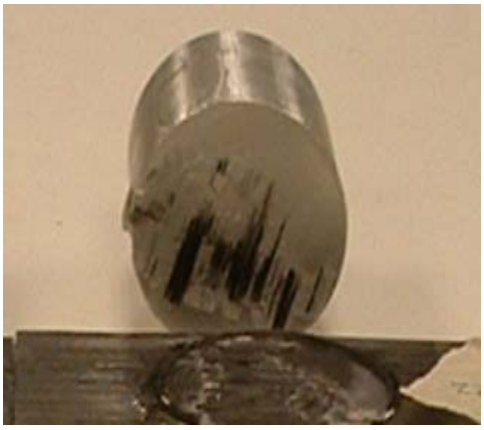

Figure 7. A failed tensile test sample.

and the HEI 535 resin system until the desired composite thickness was achieved. After trying several different techniques, it was found that the most successful method consisted of placing metal plates on the wet composite laminate and fixing them down with C-clamps. These plates helped to squeeze out any excess resin and promote fiber consolidation. Holes were cut in these metal plates where the aluminum test pieces were placed. Weight was added on top of the aluminum test pieces applying a downward force which remained during the entire cure cycle. Once cured, the test samples were cut off the mandrel with a grinder and cut into individual test samples with a table saw. Figure 8 shows the aluminum test pieces bonded to the composite laminate which is still affixed to the winding mandrel.

Section 4.2.3 – Tensile Test Procedure

As previously mentioned, ASTM D952-02, was followed as a guideline for the test procedure. However, deviations were made from the standard with regards to the test fixture, in order to allow the samples to be tested while submerged in LN_2. It is

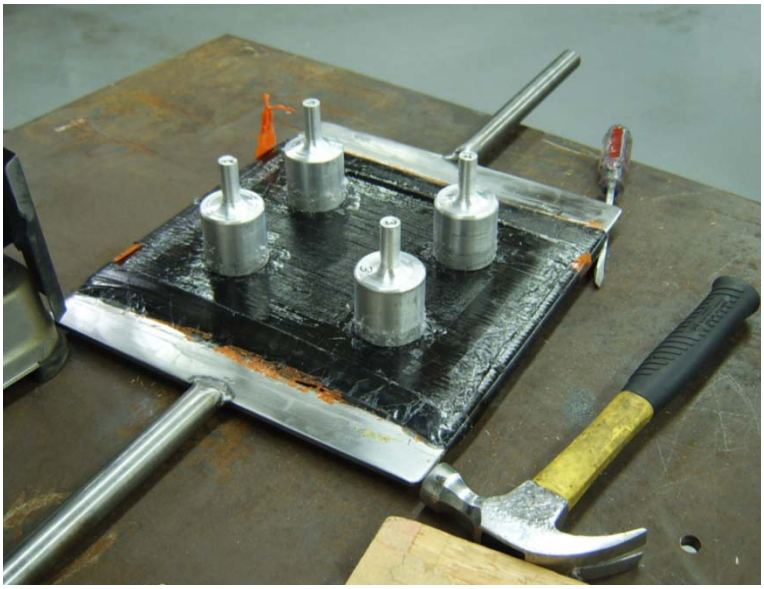

Figure 8. Laminated plate with the aluminum test pieces ready to be removed from the mandrel.

important to note that all of the cryogenic test samples were submerged in a LN_2 bath in order to allow for temperature equilibration. The samples were simply submerged in the bath; no attempt was made to try and gradually cool them down. This was done as it most closely simulates the conditions to which a cryogenic pressure vessel would be subjected to and also thought that it would be representative of a worst case scenario.

Section 4.2.3.1 – Test Fixtures

Two different test fixtures were used during the course of the tensile testing. The first model consisted of a wooden box which bolted down to the base of the tensile test machine. The test sample was situated under two 0.75 in transverse metal rods, which held it in place while the adhered button was pulled off with the tensile grips. This fixture worked well, but in some instances, it was observed that the composite would bow between the two metal rods, causing the button to peel off – thus resulting in more of a

Figure 9. The image on the left is the original test fixture, while the figure on the right shows the modified test fixture to eliminate any peeling.

peel strength than a measure of the true tensile strength. In order to rectify this problem, a cylindrical collar was fabricated to be fixed circumferentially around the aluminum test piece, which is pulled up through the center of the collar. This worked very well to avoid any peeling resulting in true tensile properties. Both text fixtures are shown in Figure 9.

Section 4.2.3.2 – Machining Test Samples

As the aluminum test samples were being used repeatedly for several series of tests, it was observed that several of the test pieces were beginning to display non-uniform curvature on the bonding surface due to the repeated sanding and buffing. In order to ensure consistent, repeatable test conditions, the bonding surface samples were parted off on a lathe, removing any concavity and ensuring that the bonding surface was true and that all of the pieces would have the same boundary conditions.

Section 4.3 – Buckling Tests

At the conclusion of the double lap shear tests and the tensile tests, the results were evaluated and the most promising combinations of prebond material, thickness and surface preparation were downselected to be used in actual pressure vessel tests.

Section 4.3.1 – Sample Preparation

The 6061 T6 aluminum liners used in the experiment featured dual ports with a volume of 7.5 L. The sidewall of the liner was chemically etched down from an initial thickness of 0.08 in to a thickness of 0.04 in. This thickness of 0.04 in was arbitrarily chosen based upon the recommendation of the company that was performing the chemical etching process.

Based on these tensile test results a test matrix was created to evaluate the most promising combinations of resin, prebond thickness and surface preparation. Additionally, a single test specimen was prepared with no special measures to prevent it from buckling. This test matrix which outlines the variables investigated is given in Table A-3 of Appendix A.

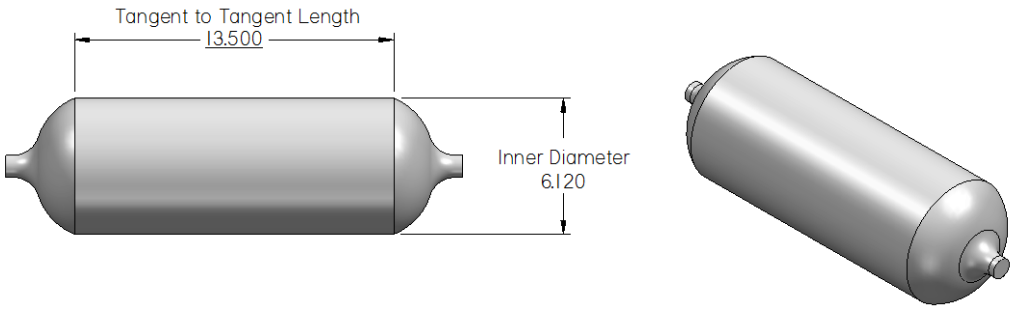

Figure 10. Aluminum liner used for the buckling tests.

Section 4.3.1.1 – Surface Preparation

The two surface preparation techniques that were evaluated in the buckling tests were grit blasting, as well as the use of the AC 130 surface etchant. The liners that were grit blast were wiped with isopropyl alcohol (IPA) in order to clean off any excess grit prior to the bonding process. Additionally, the vessels were grit blast immediately prior to the bonding process before an oxidization layer could develop on the aluminum liner.

The manufacturer's recommended application process was followed for applying the AC 130 surface etchant to the liners prior to the bonding process.

Section 4.3.1.2 – Resin Systems

Based on the results of the tensile tests, HEI 535 and AK 423 were the two resin systems downselected for use as the prebond material.

Section 4.3.1.3 – Prebond

The prebond was applied while the aluminum liner was rotating on a filament winding machine in order to achieve a uniform, consistent thickness. The prebond was allowed harden at ambient conditions and then the vessels were cured at an elevated temperature. The prebond on each of the aluminum liners were sanded prior to the application of the composite overwrap. Diametric measurements were taken before and after the application of the prebond in order to ensure that the desired thicknesses were achieved. Both thick (0.015 in) and thin (0.005 in) prebond thicknesses were evaluated. An aluminum liner following the prebond application is seen in Figure 11. Aluminum liner prepared with the prebond.

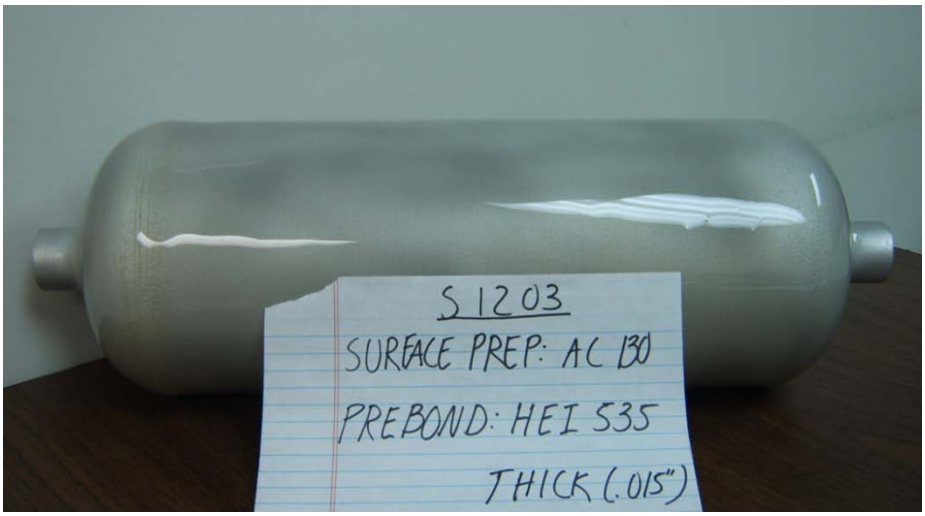

Figure 11. Aluminum liner prepared with the prebond.

Section 4.3.2 – Filament Winding Process

For the bond tests, TR 50 S graphite fiber was used because of its low cost and availability. It is not a high performance fiber and the probability that this fiber would be used in actual aerospace applications is low. However, for the buckling tests, a high modulus, high performance fiber designated as IM7 was used. Manufactured by the HEXCEL Corporation, IM7 graphite fiber was used along with the HEI 535 resin system to wet wind the vessels. The wind pattern configuration consisted of four consecutive hoop patterns at a wind angle of 88 degrees, followed by two helical patterns at a wind angle of +/- 17 degrees. This wind pattern has been previously used by HEI engineers and has an associated cryogenic burst pressure of approximately 4000 psi.

At the completion of the winding process, a compaction tape was wound around the vessel in order to promote fiber consolidation and squeeze out any excess resin.

Figure 12. Filament winding of the buckling test specimens.

The vessels were then cured at an elevated temperature according the manufacturer's recommended cure profile. This winding process is outlined in Figure 12. Filament winding of the buckling test specimens.

Section 4.3.3 – Test Procedure

The buckling tests were performed at the HEI test facility, located in Brigham City, UT. The vessels were filled with liquid nitrogen and pressurized up to 3000 psi where the pressure was held for one minute, and then depressurized. This pressure was determined by an HEI design engineer to be the autofrettage pressure associated with the aforementioned fiber layup used for these test samples. The autofrettage process consists of pressurizing the vessel to a high enough pressure to plastically deform the aluminum liner. When the pressure is relieved, the elastic recovery of the composite overwrap forces the now cold-worked aluminum liner into a compressive state, with an accompanying compressive residual stress. Figure 13 illustrates HEI's cryogenic test setup.

Figure 13. The left image illustrates the cryogenic test setup located at HEI's test facilities in Brigham City, UT. The image on the right shows a vessel that has just undergone the autofrettage process.

Section 4.4 – Impact Testing

In addition to the bonding tests, the scope of the contract also included impact testing. The Phase I portion of this contract included some introductory impact tests of both neat resin samples as well as composite laminates. These preliminary tests indicated that urethane resins with their low modulus outperformed epoxy resins in a cryogenic environment. Additionally, it was observed that a hybrid composite laminate consisting of 50% carbon fibers and 50% aramid fibers performed much better than the all-carbon laminates. Based on these results, it was determined that more comprehensive tests be conducted in an effort to find the optimum amalgamation of the two fiber types for varying levels of impact energy.

Naval Ordinance Laboratory (NOL) rings were used for the impact testing. These test samples simulate the cylindrical geometry of a pressure vessel. The test procedure consisted of two parts. The test sample consisted of first loading the ring onto a special fixture and impacting it while submerged in LN_2 with a Charpy impact head. Then, the

damaged ring would then be pulled to failure in a tensile test performed in accordance with ASTM D2290-04.

Section 4.4.1 - Sample Preparation

A metallic tube of representative diameter was treated with a release agent, and then subsequently filament wound with various fiber and resin systems. Each of the 5 layers were oriented with the fiber direction perpendicular to the axis of the tube. Off-axis angled layers were not included as they could result in warping and also adversely affect the boundary conditions. The entire tube was then cured at an elevated temperature and then the composite overwrap was removed from the tube.

Once removed from the mandrel, the composite tube was cut into individual NOL rings using a pulse laser. The optimal pulse frequency, pulse duration, power setting, and tube revolution speed were determined empirically. As seen in Figure 14, a fixture that holds and rotates the composite tube was built to assist in the cutting process. The laser cutting process resulted in reliable and repeatable cuts for all of the fiber combinations tested, with no sign of delamination. Several other abrasive cutting techniques were evaluated; however each resulted in considerable fraying and fiber damage to the test samples.

Section 4.4.1.1 - Fiber

The same IM7 graphite fiber was used during the impact testing. Additionally, zylon aramid fiber developed by Toyobo was downselected for testing to supplement the brittle carbon fibers under impact loading.

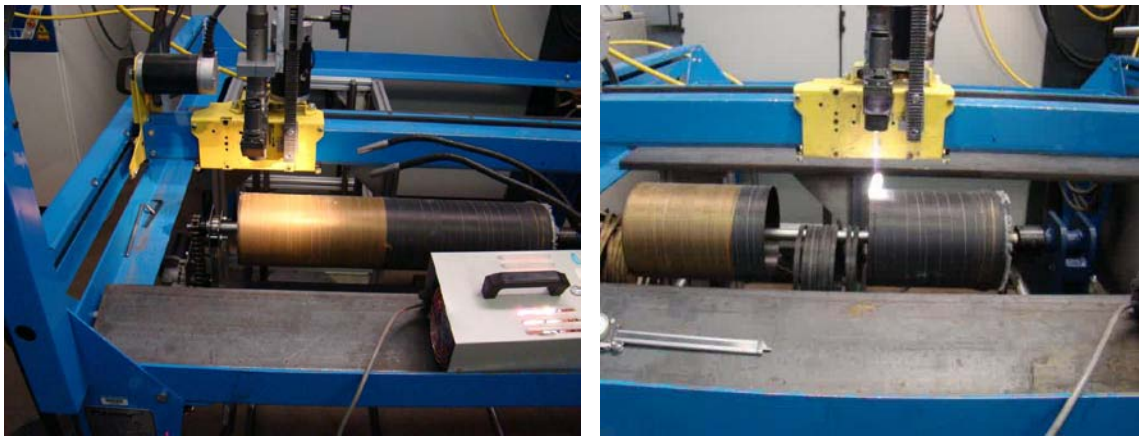

Figure 14. NOL Ring cutting procedure.

Section 4.4.1.2 – Resin Systems

Three different resin systems were evaluated including HEI 535, AK 423, as well as Epon 828. Both HEI 535 and AK 423 performed well during the tensile testing. In a prior NASA contract, HEI engineers discovered that the Epon 828 resin system performed well when used in conjunction with the zylon fiber and so it was also included into the test matrix.

Section 4.4.1.3 – Fiber Layup

The prescribed NOL layup consisted of five layers. The following fiber combinations were evaluated for each of the different resin systems:

- All IM7
- 3 IM7 / 2 Zylon
- 2 IM7 / 3 Zylon
- All Zylon

Section 4.4.2 – Test Procedure

Section 4.4.2.1 – Charpy Impact Testing

The first stage of the testing is to impact the samples. The objective of the impact is to initiate damage in the NOL ring in order to better understand how the fiber-reinforced polymers behave after being damaged. The damage expected from the impact included fiber pull out, fiber breakage, fiber/matrix debonding, delamination, and matrix/fiber crushing. As outlined in the test matrix illustrated in Table A-4 of Appendix A, the test samples were subjected to either a high or low level of energy (where high is defined as 75% of the rings impact breaking energy at cryogenic temperature and low defined as 25% of impact breaking energy). These samples were then compared with test samples that had not been impacted in order to obtain a measure of the degradation due to the impact.

In order to determine the high and low impact energy levels, a sacrificial ring was used to find the amount of energy required to completely sever the ring in a Charpy impact test. The Tinius Olson 92T Charpy impact test machine calculates the breaking energy to be the difference between the maximum potential energy of the pendulum mass before and after impact.

In order for the test machine to accommodate the NOL rings, a cylindrical aluminum anvil was designed. The ring was placed on the anvil and secured using a clamping device as seen in Figure 15.

As some of the rings warped during the cutting process, care was taken to mount the ring so that the inner face of the ring was coincident with the curvature of the

Figure 15. Modified Charpy impact test anvil.

mounting anvil ensuring the Charpy head to be square upon impact as seen in Figure 16. The impact point was marked on each ring.

Additionally, the Charpy impact test machine was fitted with a wooden enclosure which was filled with LN_2 up to the base of the test fixture to ensure the ring remained at the desired temperature during the impact procedure. As previously mentioned, prior to being impacted, both the rings as well as the anvil were submerged in the LN_2 for a minimum of one hour to ensure temperature equilibration.

Section 4.4.2.2 – Tensile Tests

ASTM D2290-04, Standard Test Method for Apparent Hoop Tensile Strength of Plastic or Reinforced Plastic Pipe by Split Disk Method, was followed as a guideline for the tensile tests conducted on the damaged NOL rings [17]. Deviations from the standard were made to allow the rings to be tested at cryogenic temperatures.

Figure 16. Charpy impact test setup.

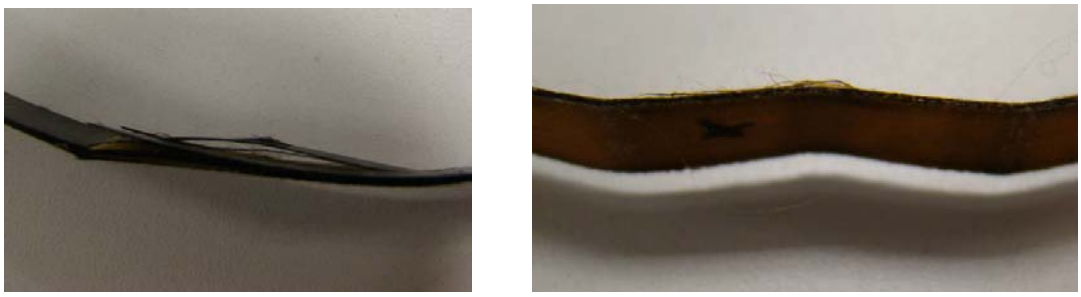

Figure 17. These images illustrate the level of damage associated with a high energy impact for two different composite layups.

As with the impact tests, a fixture was built to house the test samples so that they could tested while submerged in LN_2 illustrated in Figure 18.

Care was taken when loading the test sample to ensure that the ring was situated so that the point of impact was oriented in the same spot each time, situated at the interface where the fixtures separate. The improvised cryostat was drained and filled each time to ensure that the impacted section of the ring was submerged during the

Figure 18. The image above illustrates the improvised cryostat that was designed to allow the NOL test rings to be submerged in LN_2 during the tensile tests.

course of the test. Figure 19 illustrates the test fixtures that were designed and machined to accommodate the NOL ring during testing.

It is important to note that the split-disc tensile method does induce a bending moment in the NOL ring at the plane of speration between the disc halves. Due to the bending moment, the true tensile strength of the ring is not obtained, however, the values obtained are still sufficient for comparison purposes.

Figure 19. The images above show the NOL ring loaded on the split disk fixture ready for testing.

CHAPTER 5

RESULTS

The following sections report on the test results for the testing procedures outlined in Table 3. The test matrices for each series of testing with the actual test data are given in Appendix B.

Section 5.1 – Double Lap Shear Test Results

The double lap shear tests were invaluable in helping to identify several trends in the data, namely that the HEI 535 outperformed the urethane resin system at both ambient and cryogenic temperature when subjected to a state of shear. As seen in Figure 20, both resin systems performed best with a thin bondline at ambient temperature, while at cryogenic conditions, the thick bondline performed slightly better than the thin. Although not illustrated in the graph, it was found that the surface preparation had no discernable impact on the test results. It was also observed in a limited number of samples that some of the carbon fiber would come off on the aluminum test piece while on most samples, there was no fiber that adhered to the aluminum as seen in Figure 21.

It should be noted that the urethane did not seem to cure properly in these specimens. The adhesive remained sticky after post curing and cooling to ambient. This occurrence was noted in several of the urethane samples despite extra care being taken when measuring, mixing and curing the resin system.

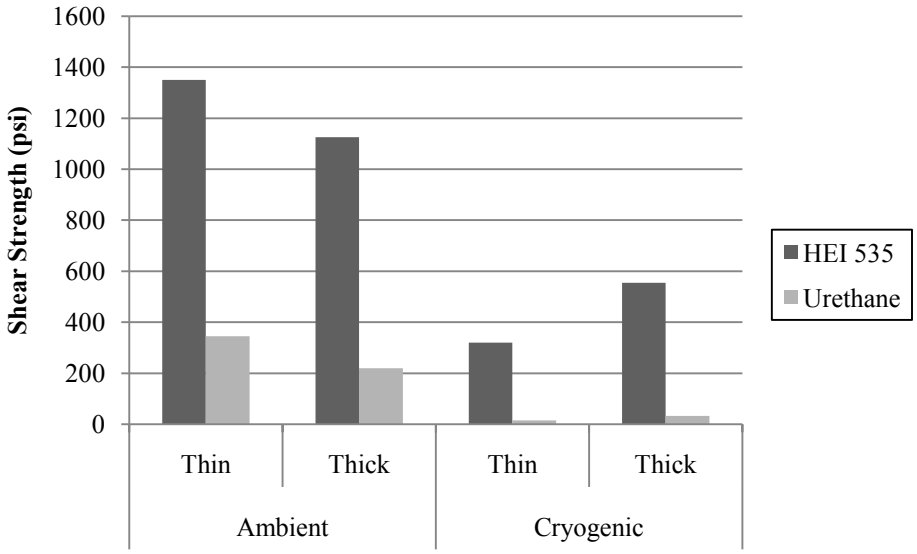

Figure 20. Double Lap shear test results.

Section 5.2 – Tensile Test Results

Section 5.2.1 – Bonding to a Cured Laminate

The initial iterations of the tensile tests were performed by bonding the aluminum test pieces to already cured composite laminates. All of the variables mentioned in the previous sections were investigated except for the prebond. For these tests, the bondline thickness between the aluminum test piece and the cured laminate was controlled using shims during the bonding process.

Section 5.2.1.1 – Ambient Test Results

Based on the ambient test results, it was discovered that the bondline thickness as well as the surface preparation did not seem to have any discernable difference on the performance of the samples.

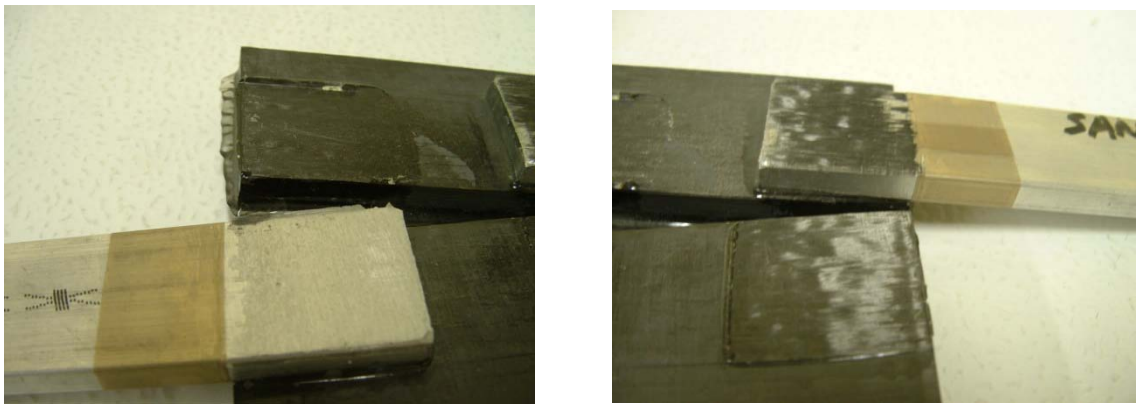

Figure 21. Failed Double Lap shear test samples.

The samples prepared with the West 105 adhesive performed very poorly. In each case, the adhesive failed to bond to the aluminum.

The urethane samples produced very inconsistent results. It was observed that during the test, failure would occur at one point and then the bond would "unzip" around the circumference of the aluminum test piece. As with the West 105 samples, failure occurred due to the bond to the aluminum. Additionally, as it was originally noticed during the double lap shear testing that some of the samples were still tacky at the bond interface.

Alternatively, the samples prepared with the Epon 828 resin system failed at the composite interface leaving a considerable amount of fiber adhered to each aluminum test piece. The different types of failure are illustrated in Figure 22.

The HEI 535 samples performed the best, achieving loads large enough that in some cases the composite laminate would start to bow considerably. Once the laminate began to bow, the button would then begin to peel off mimicking more of a peel test as opposed to a true tensile test. It was for this reason the text fixture was modified to

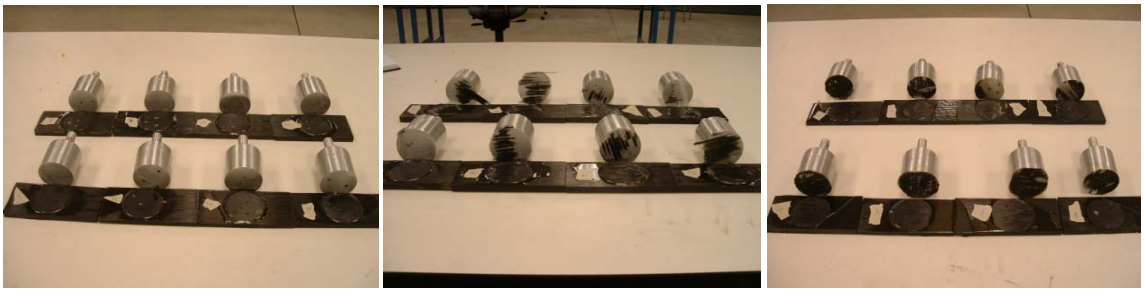

Figure 22. Failed tensile test samples.

include the cylindrical collar as described in Section 4.2.3.1 (see Figure 9). While the bond to the aluminum failed with both the urethane and West 105 samples, it was observed with the HEI 535 samples that it the bond to the composite that would fail, leaving pieces of the composite still adhered to the aluminum test piece following the test. The tensile results for the ambient tests are illustrated graphically in Figure 23.

Section 5.2.1.2 – Cryogenic Test Results

The exact same test matrix that was used for the ambient tests was repeated for the cryogenic tests. Care was taken to prepare the test specimens under the same conditions without altering any of the variables.

The most notable finding from these tests was the poor performance of certain resin systems at cryogenic temperatures. For the West 105 resin system, more than half of the samples broke in the cooler of LN_2 during the equilibration period prior to testing.

The Epon 862 samples also performed very poorly at cryogenic conditions as illustrated in Figure 24. This behavior was not entirely unexpected however as neither of these resin systems are designed for use in a cryogenic environment.

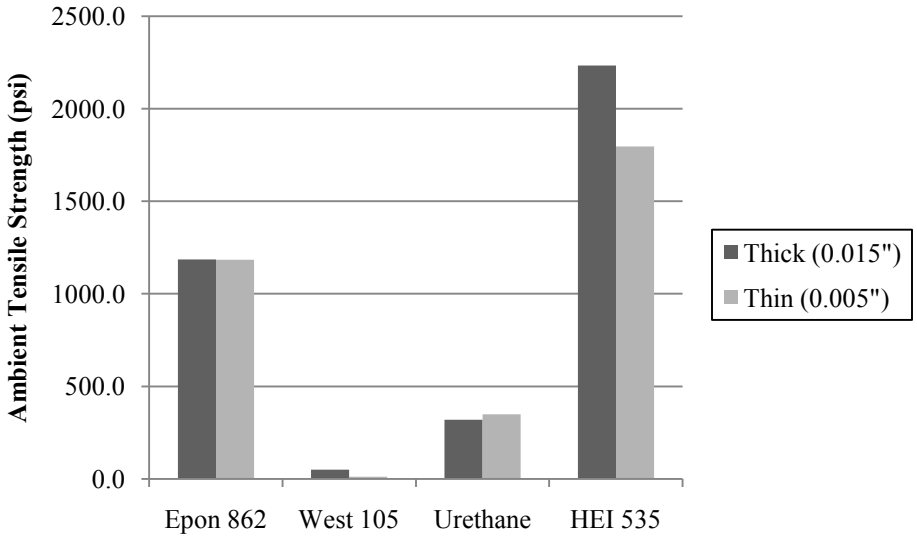

Figure 23. Ambient tensile test results - bonding to and already cured composite laminate.

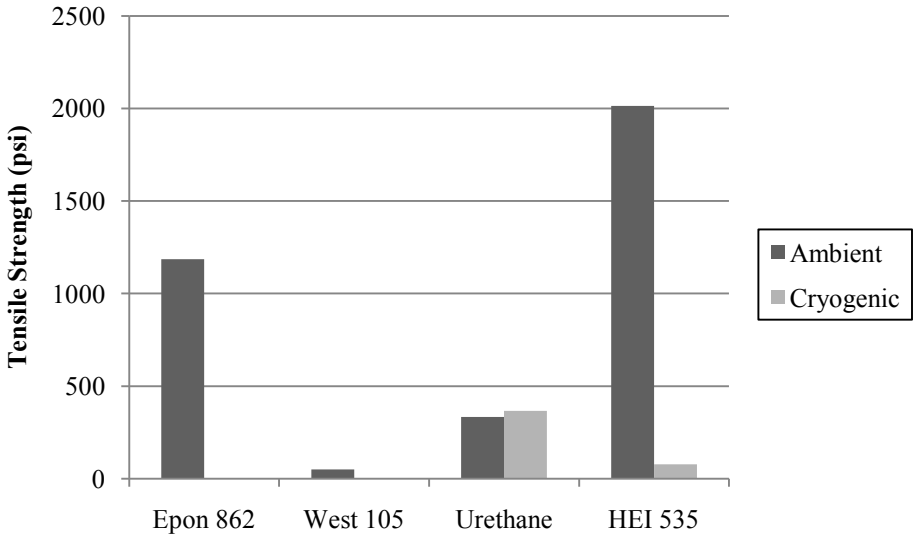

Figure 24. Cryogenic tensile results – resin comparison.

For the HEI 535 resin system, the samples with a thick bondline performed poorly with no distinguishable difference between the “abrasive” and “as machined” finishes.

For the samples with a thin bondline, the ones with an demonstrated a higher tensile strength.

The urethane samples performed the best out of all the resin systems tested. Opposite from the HEI 535 specimens, the thick bondline samples performed much better than the thin as seen in Figure 25. Again the surface finish didn't seem to have any effect on the performance.

For all the adhesives tested, it was the bond to the aluminum that failed; however several of the urethane samples did pull off some composite.

Section 5.2.2 – Bonding to a Co-Cured Laminate

While the tensile tests in which the aluminum test fixture was bonded to an already cured laminate were very helpful in identifying how each of the resin systems would perform in a cryogenic environment, they did not accurately replicate the bonding conditions of a COPV. The next series of tests introduced applying the aluminum test piece while the

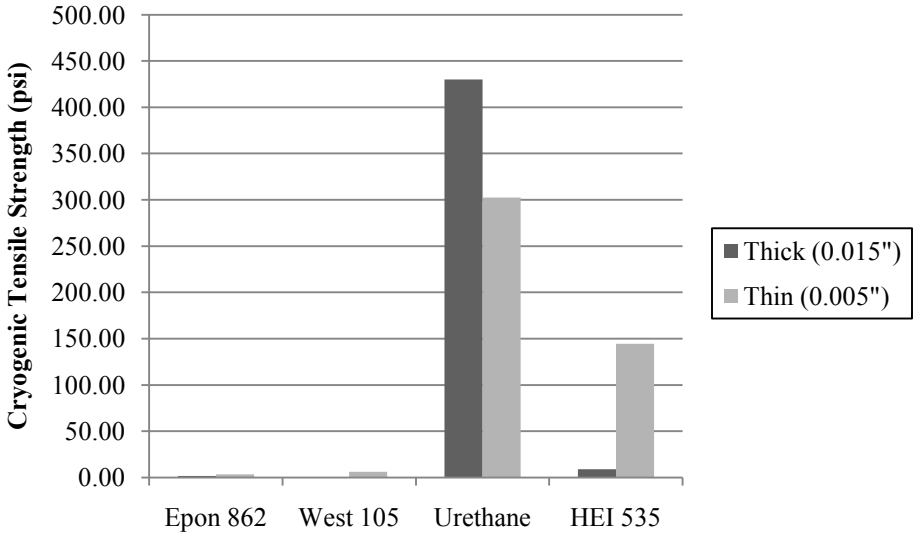

Figure 25. Cryogenic tensile results - bondline thickness comparison.

composite laminate was still wet, and co-curing the samples together. It was believed that this would be more representative of the conditions that occur in a pressure vessel.

Section 5.2.2.1 – Resin Systems

At this point, due to the poor performance of the West 105 resin system at both cryogenic and ambient temperatures, and the Epon 862 at cryogenic temperatures, both were eliminated from further evaluation.

As mentioned earlier, in several cases, the bond surfaces of the urethane samples would still be tacky following the test. Several corrective actions were taken to try and overcome this problem including increasing the cure time, increasing the mixing time to ensure the homogeneity of the two part system prior to application, and the use of an electric mixer rather than mixing by hand. None of these actions seemed to help so the formulators of this experimental resin system at NASA MSFC were contacted. They were aware of this issue and had also observed this phenomenon. During the course of the conversation, they informed us of another recently developed experimental urethane resin system and asked that we discontinue the use of the previous urethane and begin testing the new system which is designated as AK 423.

As previously mentioned, AK 423 is another low modulus, experimental urethane resin system formulated by NASA MSFC for use in low temperature applications. Using the new cylindrical collar test fixture, extensive testing was performed at both ambient and cryogenic conditions evaluating the new AK 423 as well as HEI 535.

Section 5.2.2.2 – Prebond

It was during these tests where the aluminum test fixtures were applied to a wet composite laminate that the prebond was introduced, as described in Section 4.2.1.3. As seen in Figure 26, the prebond had a dramatic positive effect on the overall tensile strength of the test samples for both ambient and cryogenic conditions.

Section 5.2.2.3 – Surface Preparation

During the course of these tests, it was observed that with both the AK 423 and HEI 535, in every instance, the bond would fail at the prebond-aluminum interface (see Figure 6) for both the 'as machined' and 'sanded' surface preparation methods. Based on this observation, it was determined that more aggressive measures needed to be taken to enhance the bonding surface area. Therefore, the surface preparations of grit blasting and the use of a surface etchant were investigated.

A new series of test samples were prepared with the new surface preparation techniques as well as the other previously included variables. As these samples were tested, instead of failing the bond at the prebond-aluminum interface, failure occurred at the prebond-composite interface. However, the tensile strength was much lower than the tests when the failure mode was at the prebond-aluminum interface.

The reason for this anomaly was determined to be in the prebond preparation process. Following the application of the surface etchant and the grit blasting processes, the metal shims that control the bondline thickness were adhered to the bottom of the aluminum test fixtures and the samples were placed in a resin bath. Originally, the fixtures were placed in the bath, the resin was cured, and then the excess resin was cut from around the

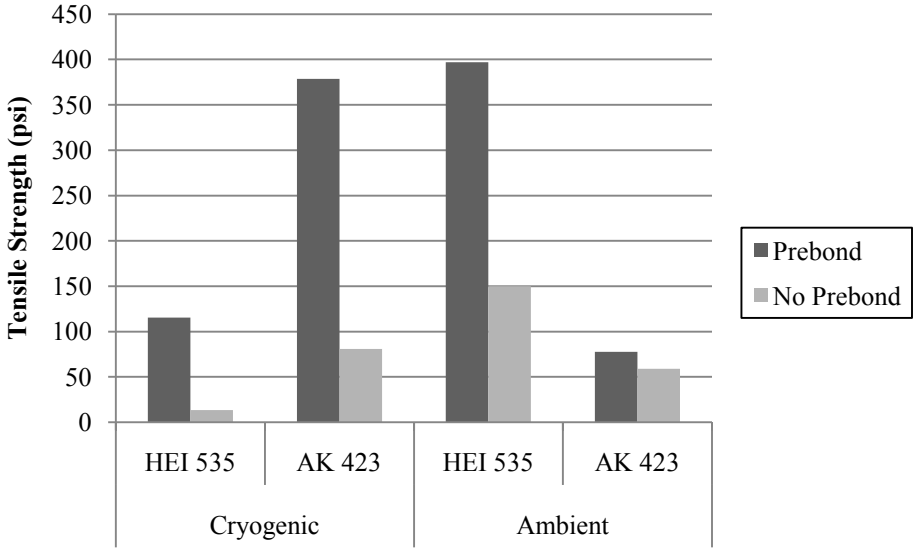

Figure 26. Bonding to a co-cured laminate test results - prebond comparison.

edges of the prebond. The prebond was then sanded down to achieve the proper thickness. However, in the aforementioned case when the surface etchant and grit blasting surface preparation techniques were first introduced, weight was added to the top of the buttons to achieve the proper prebond thickness, thus eliminating the tedious and time consuming process of having to sand the prebond after curing the resin. The previously mentioned irregularity where the bond to the composite failed at a lower strength is attributed to the fact that this finish sanding process was eliminated from these samples. In order to confirm this hypothesis, an identical set of test samples was prepared; however this time the traditional method of preparation was followed and the prebond was sanded. These tests resulted in some of the highest strengths yet achieved. It was very interesting to note that failure primarily occurred at the prebond-aluminum interface for the majority of the samples prepared with the grit blasting surface preparation technique. However for the samples prepared with the surface etchant, the

bond to the composite or a mixed mode of failure occurred for the majority of the test specimens.

The importance of sanding the prebond is considered to be very valuable information and its dramatic effect is illustrated in Figure 27.

A similar trend as depicted in Figure 27 was also noticed for the AK 423 resin system.

Another interesting trend noticed for the HEI 535 samples, was the minute difference in the performance of the thick and thin prebond samples as seen in Figure 28. For both the samples prepared with the AC 130 surface etchant as well as the samples prepared with a grit blast surface preparation, the thick prebond slightly outperformed the

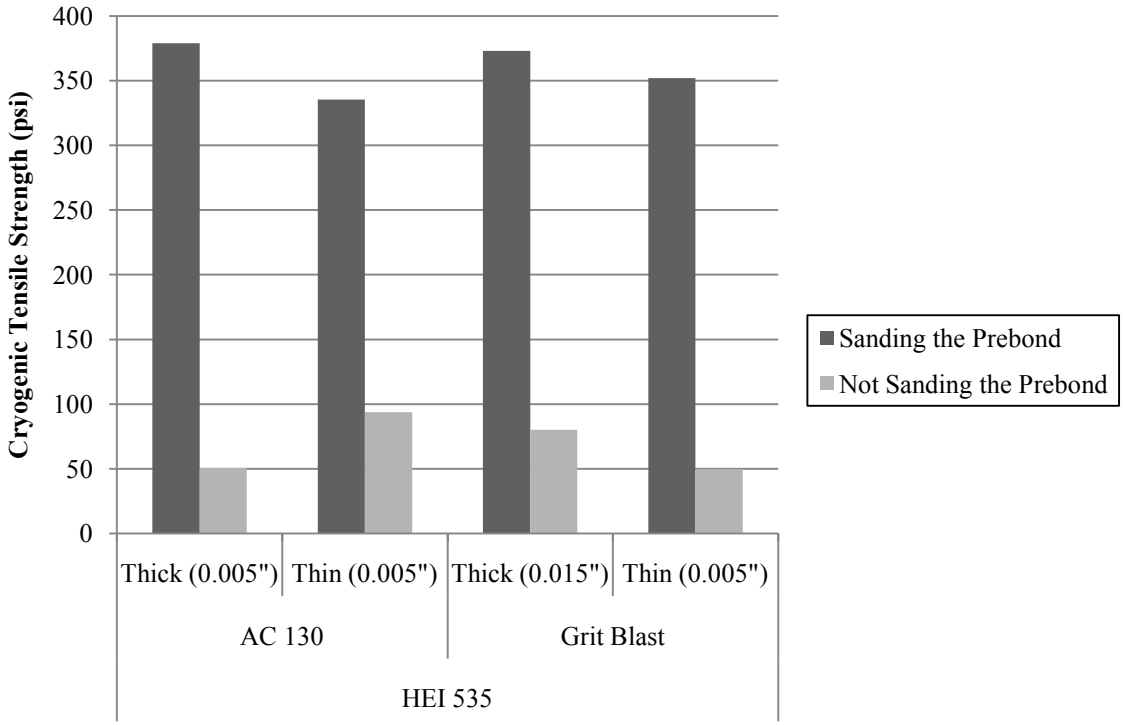

Figure 27. Bonding to a co-cured laminate tensile test results - effect of sanding the prebond.

thin. Alternatively, the AK 423 samples prepared with a thin prebond significantly outperformed those with a thick prebond.

Also illustrated in Figure 28 is that the HEI 535 samples prepared with the AC 130 surface etchant only performed slightly better than those prepared with the grit blast surface preparation.

The surface preparation also played a key role in the mode of failure. For both the 'as machined' samples, as well as the samples that were sanded with course sandpaper, failure would always occur at the prebond-aluminum interface as seen in the image on the left in Figure 29. The more aggressive surface preparation techniques resulted in increased bond strength as well as a mixed failure mode as illustrated in the image on the right in Figure 29. This mixed mode of failure was determined to be ideal

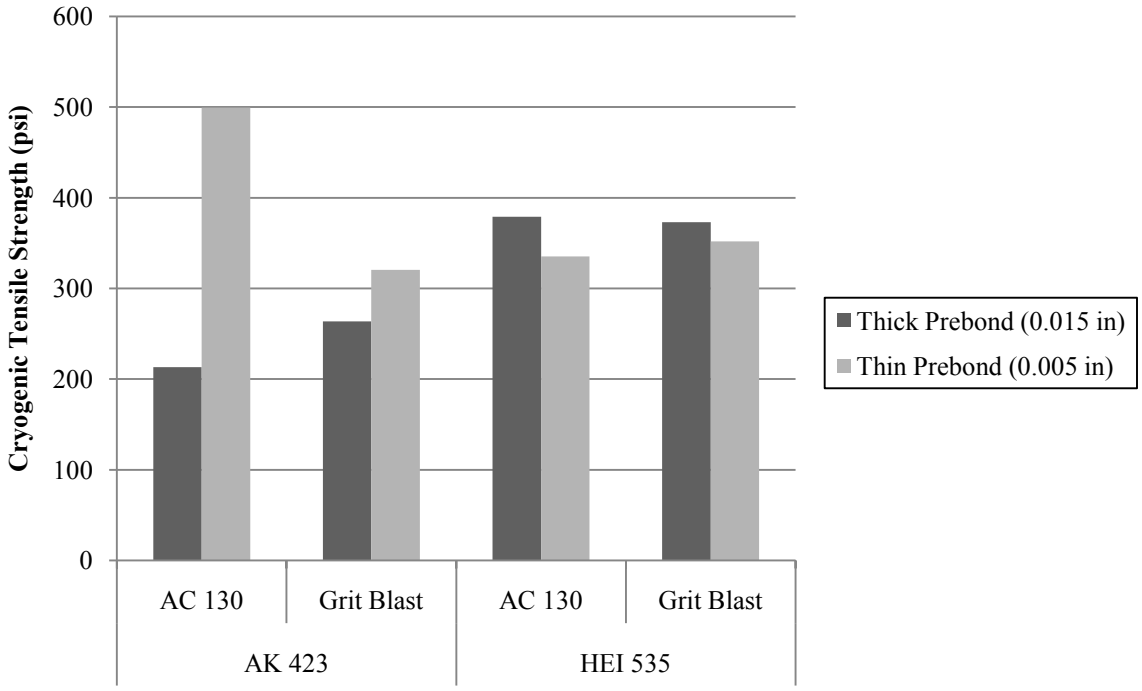

Figure 28. Bonding to a co-cured laminate tensile test results.

as the bond between the prebond and the aluminum as well as the bond at the adhesive-composite interface failed simultaneously.

Unfortunately, there was not time to perform enough tests build a sufficiently large database, and these results are based upon a limited test population. It is encouraged that additional tests be conducted evaluating the AC 130 and grit blast surface preparations in order to further validate the results and trends outlined in this section.

Section 5.3 – Buckling Test Results

All of the vessels in the test matrix were subjected to the test procedure outlined in the previous section. Surprisingly, none of the vessels showed any signs of buckling, not even the vessel without any prebond or surface preparation.

Section 5.4 – Impact Test Results

The breaking energy for each of the fiber configurations was found for each resin system and is listed in Table 4.

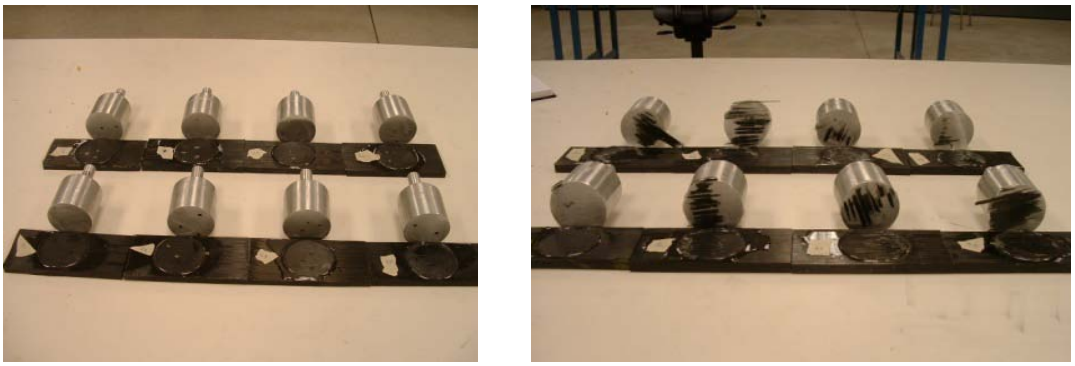

Figure 29. Failed co-cured tensile test samples.

It is important to note that the Charpy impact test machine could not break the all zylon rings irrespective of the resin system, despite loading it with all of the available weights. The maximum amount of energy that could be generated was approximately 45 in-lbs which is why there is little variation in the all zylon breaking energy data. As illustrated however, is that HEI 535 and AK 423 performed comparably, with a considerably higher breaking energy than the Epon 828 resin system.

Table 5 summarizes the average NOL ring tensile strength after being subjected to a high impact for the HEI 535 resin system. This value is then compared against the strength of a ring that was not impacted in order to get a measure of the degradation due to the impact.

Table 4. Average Cryogenic NOL Ring Breaking Energy

Layup	HEI 535 (in-lbs)	AK 423 (in-lbs)	Epon 828 (in-lbs)
All Carbon	3.98	2.08	2.72
3 Carbon / 2 Zylon	37.04	32.84	25.82
2 Carbon / 3 Zylon	42.01	41.85	30.23
All Zylon	44.57	44.707	45.33

Table 5. Average Cryogenic NOL Ring Tensile Strength for the HEI 535 Resin

Fiber Layup	Impact Energy	Post Impact Tensile Strength
All IM7	High	5%
3 IM7/2 Zylon	High	74%
2 IM7/3 Zylon	High	80%
All Zylon	High	93%

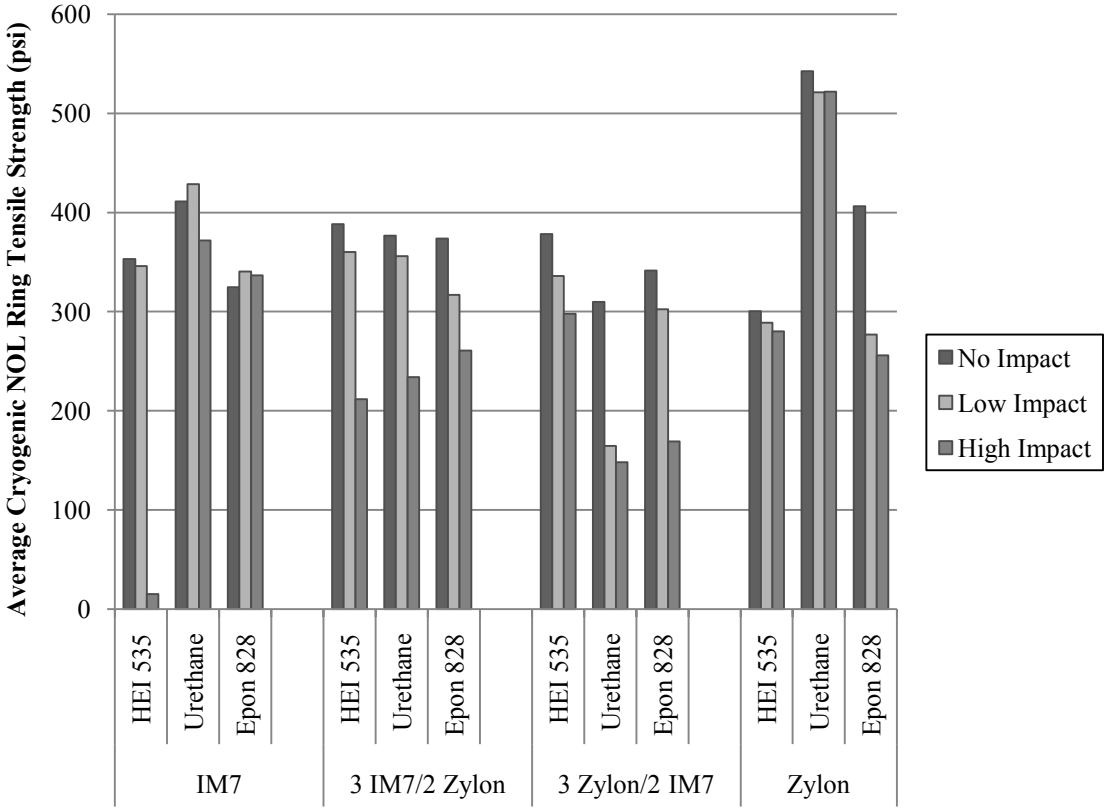

Figure 30. Average NOL Ring tensile strength for each of the layup configurations and resin systems.

As seen, there is a dramatic increase in strength as more layers of zylon are added to the composite layup. Figure 30 illustrates the overall performance of the fiber combinations and resin systems.

It is important to note that some of the data in this graph can appear misleading, particularly the high and low impact - all IM7 samples. Due to the extremely low breaking energy of the all IM7 samples (2-4 in-lbs depending on the resin system), the resulting high and low impact energy values (75% and 25% of the breaking energy) were so small, that often it was not enough to do any damage at all to the NOL ring. This means that several of the high and low impact samples were subjected to such a low level of impact, that it was as if they were not impacted at all, which is why there is very little

degradation illustrated in the graph for the all IM7 samples. The all IM7 carbon fibers behaved in an extremely brittle manner, and that any substantial amount of impact would prove catastrophic.

Additionally, the 3 Zylon/2 IM7 layup with the urethane experienced a manufacturing defect in the outer 2 layers. Due to the extremely short pot life of the experimental urethane, the mandrel was wound with dry fiber then the resin had to be brushed on afterwards. During this application process, the outer layer of zylon meshed together with the lower carbon layer. This resulted in a cylindrical laminate that was no longer symmetric which introduced bend-extension and bend-twist coupling into the test samples. The additional stresses caused by the undesired coupling terms decreased the failure load.

CHAPTER 6

BUCKLING ANALYSIS

After the pressure vessels that were tested failed to demonstrate any signs of buckling, a analytical analysis was commenced in order to determine the critical parameters required for buckling to occur. It was initially believed that as the vessel is internally pressurized during the autofrettage process, it may be possible to stress the aluminum liner such that the plastic deformation is sufficient to demonstrate an axial buckling mode in the liner due to the elastic recovery of the composite overwrap during depressurization. This analysis provides valuable insight into important parameters such as liner sidewall thickness and length, composite layup orientation, and the internal pressure necessary to achieve the critical buckling load

It is important to note that this analysis method uses many approximations and assumptions. It is by no means a "ready for market" solution method. This analysis was developed outside the scope of the contract in order to get a better idea of what conditions are necessary for buckling to occur. Additionally this solution only investigates and accounts for axial buckling. It is possible that circumferential buckling could also occur, but this mode was not considered in the study that is described in the subsequent sections.

The flowchart illustrated in Figure 31, outlines the processes of this buckling analysis.

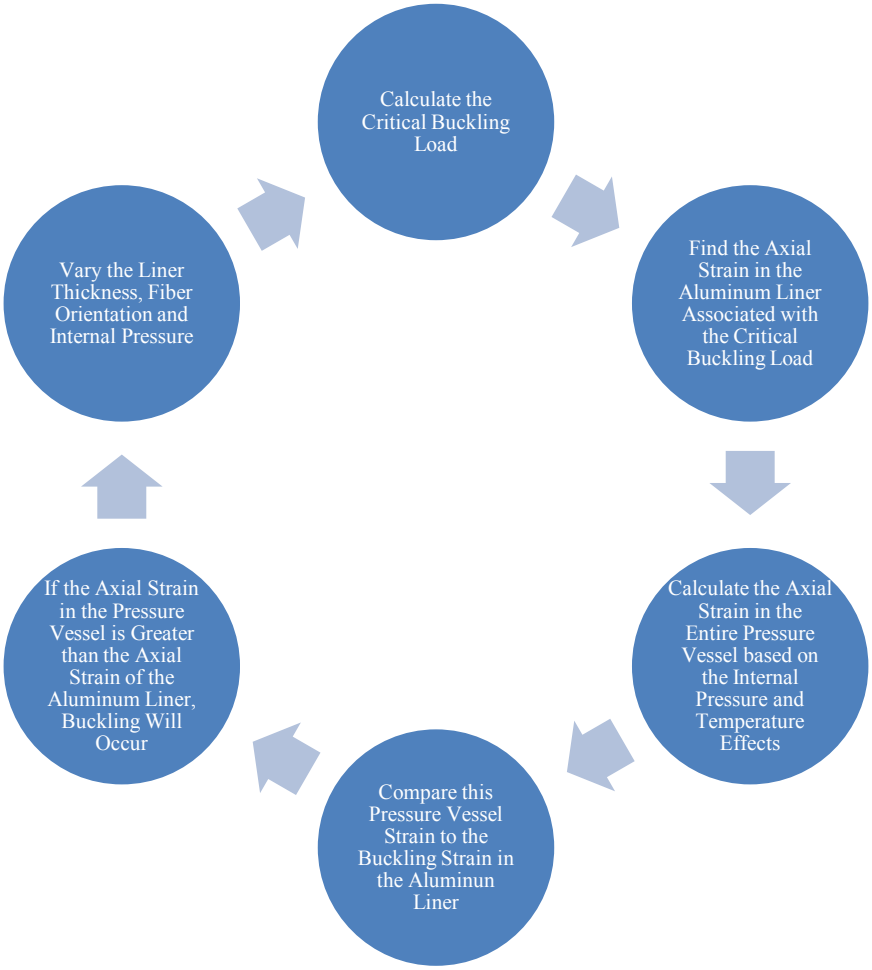

Figure 31. Flowchart outlining the different processes of the buckling analysis.

Section 6.1 – Calculating the Critical Buckling Load

The buckling analysis for a thin walled, isotropic cylinder due to an axial loading and internal pressure may be found in a variety of texts such as [18].

For the case of axial compression (as would be experienced in the aluminum liner of a pressure vessel), the critical buckling load is given by the following equation

$$q_2 = \{(1-\upsilon)\lambda^4 + k[(\lambda^2+m^2)^4 - 2(\upsilon\lambda^6 + 3\lambda^4 m^2 + (4-\upsilon)\lambda^2 m^4 + m^6) + 2(2-\upsilon)\lambda^2 m^2 + m^4]\}\,[\lambda^2(\lambda^2+m^2)^2 + \lambda^2 m^2]^{-1} \quad [1]$$

where

$$\lambda = \frac{n\pi a}{l} \quad [2]$$

$$k = \frac{K}{Da^2} \quad [3]$$

$$K = \frac{Et^3}{12(1-\nu^2)} \quad [4]$$

$$D = \frac{Et}{1-\nu^2} \quad [5]$$

and

$a =$ inner radius
$l =$ overall length
$n =$ integer
$m =$ integer
$t =$ thickness
$q_2 =$ axial load / length
$\upsilon =$poissons ratio

The critical buckling load per unit length q_2, is largely dependent on the cylinder sidewall thickness, radius and length. By multiplying the critical buckling load by the cylinder circumference, the total buckling force can be calculated. The critical buckling load was calculated using Equations 1-5 for several different liner thickness values as seen in Table 6. Although the length contributes significantly to the liner buckling, only the liner sidewall thickness was varied in this analysis. Due to the fact that HEI had already procured several of the standard test evaluation vessels, there could be no variance in the length; however the original cylinder sidewall thickness of 0.080 in could be reduced through a chemical etching process.

Table 6. Critical Buckling Load for Varying Liner Thicknesses

Critical Buckling Load		
Liner Thickness (in)	q_2 (lbf/in)	Total Load (lbf)
0.015	455.69	8761.34
0.0175	601.44	11563.60
0.02	779.4	14985.16
0.0225	994.17	19114.44
0.025	1250.36	24040.09
0.03	1840.75	35391.24

Section 6.2 – Strain Required for Buckling

The axial strain associated with each critical buckling load listed in Table 6 was then calculated using an elasticity solution for the aluminum liner. A triaxial stress state with axisymmetric boundary conditions was considered. The computer program described in Section 6.3.2 was used to calculate the actual values using the material properties for just the aluminum liner in the accompanying input file.

It is important to note that there is a very large discrepancy between the yield strength of 6061 aluminum verses 6061 aluminum with the T6 heat treatment. Even though the aluminum liner used in the buckling tests had the T6 heat treatment, the properties used in the analysis to find the elastic strain are based on 6061 aluminum with no heat treatment. As the recrystallization temperature of aluminum is 176 °F, it was assumed that during the cure cycle (which sustains a temperature of 185 °F for 20 hours) the grain structure of the aluminum returned to its undeformed state. The aforementioned aluminum properties can be found in Appendix C.

Table 7. Critical Buckling Conditions for Varying Liner Thicknesses

Critical Buckling Conditions for the Aluminum Liner			
Liner Thickness (in)	Plastic Strain (με)	Elastic Strain (με)	Total Liner Strain (με)
0.015	2755	730	3485
0.0175	3115	730	3845
0.02	3530	730	4260
0.0225	4000	730	4730
0.025	4528	730	5258
0.03	5550	730	6280

The total strain associated with the critical buckling load for each of the different liner geometries is given in Table 7.

This total strain calculated based on the critical buckling load represents the strain necessary to induce plastic deformation, and subsequent buckling for the aluminum liner.

Section 6.3 – Calculate Pressure Vessel Strain

Once the axial strain associated with the buckling of the aluminum liner was found, the next step of the buckling analysis was to calculate the axial strain for the entire pressure vessel. The equations used to calculate these strains are outlined in the sections below.

Section 6.3.1 – Solution Methodology

A closed form solution for a laminated composite cylinder was then employed. This solution technique uses linear elastic relationships to calculate the displacements, stresses and strains for a cylinder subjected to the following axisymmetric conditions:

a) a uniform interior pressure, p_{in}
b) a uniform exterior pressure, p_{out}
c) a uniform temperature change, ΔT
d) an axial load applied at the ends, P_x or a uniform axial strain, ε_x^o

e) a torque, T_x, or uniform angle of twist per unit length, γ^o

Only an abbreviated explanation of the solution technique is outlined in this section. For a complete presentation of this solution, see [19, 20].

The geometry of the laminated cylinder along with the cylindrical coordinates and loading are shown in Figure 32.

It is assumed that each layer is homogeneous. Also each layer may be oriented off the cylinder axial direction at an angle, ϕ, as shown

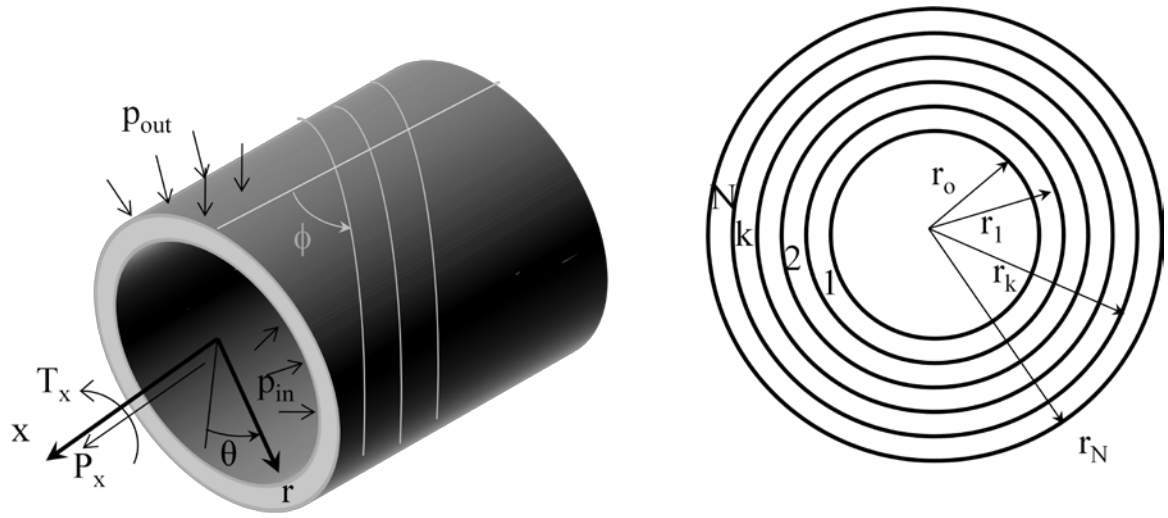

Figure 32. Geometry, loading directions, and layer numbering of an axisymmetric laminated cylinder.

Section 6.3.1.1 – Governing Equations

From the axisymmetric assumption, the strain-displacement equations may be written as

$$\varepsilon_x = \frac{du}{dx} \qquad \varepsilon_\theta = \frac{w}{r} \qquad \varepsilon_r = \frac{dw}{dr} \qquad [6, 7, 8]$$

$$\gamma_{r\theta} = \frac{dv}{dr} - \frac{v}{r} \qquad \gamma_{xr} = \frac{du}{dr} \qquad \gamma_{\theta x} = \frac{dv}{dx} \qquad [9, 10, 11]$$

and the nontrivial compatibility equations are

$$\frac{d^2\varepsilon_x}{\partial r^2} = 0 \qquad \frac{1}{r}\frac{d\varepsilon_x}{\partial r} = 0 \qquad \frac{1}{2}\frac{d}{dr}\left[\frac{1}{r}\frac{d}{\partial r}\left(r\gamma_{x\theta}\right)\right] = 0 \qquad [12, 13, 14]$$

It is assumed that the cylinder is long and all loading and geometry is axisymmetric. Therefore, the stresses are assumed to be independent of the axial direction, x, and the hoop direction, θ. The three-dimensional equilibrium equations then reduce to

$$\frac{d\sigma_r}{dr} + \frac{1}{r}\left(\sigma_r - \sigma_\theta\right) = 0 \qquad \frac{d\tau_{r\theta}}{dr} + \frac{2}{r}\tau_{r\theta} = 0 \qquad \frac{d\tau_{xr}}{dr} + \frac{1}{r}\tau_{xr} = 0 \qquad [15, 16, 17]$$

The lamina constitutive equations, including the free thermal strains, may expressed as

$$\begin{Bmatrix} \sigma_x \\ \sigma_\theta \\ \sigma_r \\ \tau_{\theta r} \\ \tau_{rx} \\ \tau_{x\theta} \end{Bmatrix} = \begin{bmatrix} \overline{C}_{11} & \overline{C}_{12} & \overline{C}_{13} & 0 & 0 & \overline{C}_{16} \\ \overline{C}_{12} & \overline{C}_{22} & \overline{C}_{23} & 0 & 0 & \overline{C}_{26} \\ \overline{C}_{13} & \overline{C}_{23} & \overline{C}_{33} & 0 & 0 & \overline{C}_{36} \\ 0 & 0 & 0 & \overline{C}_{44} & \overline{C}_{45} & 0 \\ 0 & 0 & 0 & \overline{C}_{45} & \overline{C}_{55} & 0 \\ \overline{C}_{16} & \overline{C}_{26} & \overline{C}_{36} & 0 & 0 & \overline{C}_{66} \end{bmatrix} \begin{Bmatrix} \varepsilon_x - \Delta T\alpha_x \\ \varepsilon_\theta - \Delta T\alpha_\theta \\ \varepsilon_r - \Delta T\alpha_r \\ \gamma_{\theta r} \\ \gamma_{rx} \\ \gamma_{x\theta} - \Delta T\alpha_{x\theta} \end{Bmatrix} \qquad [18]$$

where $\overline{C}_{ij}$ are the transformed stiffness terms and the off-axis coefficients of thermal expansion in terms of the on-axis coefficients of thermal expansion are

$$\alpha_x = \alpha_1 \cos^2\phi + \alpha_2 \sin^2\phi \quad \alpha_\theta = \alpha_1 \sin^2\phi + \alpha_2 \cos^2\phi \quad \alpha_r = \alpha_3 \qquad [19, 20, 21]$$

$$\alpha_{x\theta} = 2\sin\phi\cos\phi(\alpha_1 - \alpha_2) \qquad [22]$$

The displacements in an individual lamina (the k^{th} lamina) are found through clever manipulation of the stated equations and are found to be

$$u_k(x) = \varepsilon_x^o x \qquad [23]$$

$$v_k(x,r) = \gamma^o xr \qquad [24]$$

$$w_k(r) = A_1^{(k)} r^{\lambda_k} + A_2^{(k)} r^{-\lambda_k} + \Gamma_k \varepsilon_x^o r + \Omega_k \gamma^o r^2 + \Psi_k r \Delta T \qquad [25]$$

where,

$$\Gamma = \left(\frac{\overline{C}_{12} - \overline{C}_{13}}{\overline{C}_{33} - \overline{C}_{22}}\right) \quad \Omega = \left(\frac{\overline{C}_{26} - 2\overline{C}_{36}}{4\overline{C}_{33} - \overline{C}_{22}}\right) \quad \Psi = \left(\frac{\widetilde{\Sigma}}{\overline{C}_{33} - \overline{C}_{22}}\right) \qquad [26, 27, 28]$$

$$\widetilde{\Sigma} = (\overline{C}_{13} - \overline{C}_{12})\alpha_x + (\overline{C}_{23} - \overline{C}_{22})\alpha_\theta + (\overline{C}_{33} - \overline{C}_{32})\alpha_r + (\overline{C}_{63} - \overline{C}_{62})\alpha_{x\theta} \qquad [29]$$

and

$$\lambda_k = \sqrt{\frac{\overline{C}_{22}}{\overline{C}_{33}}} \qquad [30]$$

Section 6.3.1.2 – Determining Lamina Constants

The problem is now reduced to finding the constants $A_1^{(k)}$ and $A_2^{(k)}$ for each lamina and either the axial strain, ε_1° or axial force, P_x and either the angle of twist, γ° or torque, T_x. For a laminate of N laminae, there are $2N+2$ unknowns. Thus, $2N+2$ equations containing the unknowns are constructed as

$$\begin{bmatrix} K_{11} & K_{12} & \cdots & K_{1,2N+2} \\ K_{21} & K_{22} & & K_{2,2N+2} \\ \vdots & & \ddots & \vdots \\ K_{2N+2,1} & K_{2N+2,2} & \cdots & K_{2N+2,2N+2} \end{bmatrix} \begin{Bmatrix} A_1^{(1)} \\ A_2^{(1)} \\ \vdots \\ A_1^{(k)} \\ A_2^{(k)} \\ \vdots \\ A_1^{(N)} \\ A_2^{(N)} \\ P_x \text{ or } \varepsilon_x^\circ \\ T_x \text{ or } \gamma_{x\theta}^\circ \end{Bmatrix} = \begin{Bmatrix} F_1 \\ \vdots \\ F_i \\ \vdots \\ F_{2N+2} \end{Bmatrix} \qquad [31]$$

In order to then solve for these unknown values, equations are developed from the displacement and stress equilibrium conditions at the laminae boundaries. This is somewhat an exhaustive process and the details are not illustrated in this document.

Once all of the terms in the [K] and {F} matrices are found, a linear solution technique can be used to solve for the unknown values. These values can be back-substituted into Equations 23-25 to find the displacements.

Once all of the displacements have been identified, the resulting strains and stresses can be found.

Section 6.3.1.3 – Determining Lamina Strains and Stresses

Once the displacements are found the non-zero, lamina strains are identified from Equations 6-11 as:

$$\varepsilon_x = \varepsilon_x^o \tag{32}$$

$$\varepsilon_\theta(r) = A_1^{(k)} r^{\lambda_k - 1} + A_2^{(k)} r^{-\lambda_k - 1} + \Gamma_k \varepsilon_x^o + \Omega_k \gamma^o r + \Psi_k \Delta T \tag{33}$$

$$\varepsilon_r(r) = A_1^{(k)} \lambda_k r^{\lambda_k - 1} - A_2^{(k)} \lambda_k r^{-\lambda_k - 1} + \Gamma_k \varepsilon_x^o + 2\Omega_k \gamma^o r + \Psi_k \Delta T \tag{34}$$

$$\gamma_{x\theta}(r) = \gamma^o r \tag{35}$$

Although we are mainly interested in the strains, the lamina stresses can also be found from the constitutive relationships, Equation 36, put in a reduced form as:

$$\begin{Bmatrix} \sigma_x \\ \sigma_\theta \\ \sigma_r \\ \tau_{x\theta} \end{Bmatrix} = \begin{bmatrix} \overline{C}_{11} & \overline{C}_{12} & \overline{C}_{13} & \overline{C}_{16} \\ \overline{C}_{12} & \overline{C}_{22} & \overline{C}_{23} & \overline{C}_{26} \\ \overline{C}_{13} & \overline{C}_{23} & \overline{C}_{33} & \overline{C}_{36} \\ \overline{C}_{16} & \overline{C}_{26} & \overline{C}_{36} & \overline{C}_{66} \end{bmatrix}_k \begin{Bmatrix} \varepsilon_x - \Delta T \alpha_x \\ \varepsilon_\theta - \Delta T \alpha_\theta \\ \varepsilon_r - \Delta T \alpha_r \\ \gamma_{x\theta} - \Delta T \alpha_{x\theta} \end{Bmatrix} \tag{36}$$

Section 6.3.2 – Cylinder Buckling Program

A computer program was written in FORTRAN that finds the unknown coefficients $A_1, A_2, \varepsilon_x^0$, and γ^0 and incorporates a post processer to find the displacements, strains, and stresses. This conveniently allows the user to create an input file containing the cylinder geometry, material properties and loading conditions and then compiles all of the calculated stress and strain values into an output file. By putting all of the

equations into a loop, the aforementioned calculations are quickly performed for each layer of the composite tube. A copy of this program can be found in Appendix D.

Section 6.4 – Strain Comparison

After having found the axial strain for the entire pressure vessel, this value was then compared to the strain associated with the buckling of the liner. It was assumed that if an axial strain for the entire pressure vessel could be achieved during the autofrettage process that is greater than or equal to the axial strain in the aluminum liner that was calculated based upon the liner critical buckling load, then there would be a high probability that buckling could occur. This process was repeated for several different liner thicknesses as well as several different composite fiber orientations.

Section 6.5 – Buckling Analysis Results

Based on the required strain values for buckling defined in Table 7, an iterative scheme was used in order to determine the internal pressure and associated axial load necessary to achieve that axial strain for the various liner thicknesses.

Table 8 and Table 9 are based upon liner thicknesses of 0.015 in. Illustrated in each of the tables are several different composite layup orientations. Additionally tabulated are the associated thermal strains, the strain due to the internal pressure, as well as the strain due to the axial load (axial load being due to the internal pressure acting upon the pressure vessel endcaps) for the entire pressure vessel. All of these strains were summed up and then compared to the axial strain in the aluminum liner required for buckling.

From Table 7, for a 0.015 in thick liner, a value of 3485με is required for buckling. As seen in Table 8, a vessel wound with four circumferential layers of composite at a wind angle of 88°, and two helical layers at a wind angle of +/-17° would achieve a strain of 4329με when subjected to an internal pressure of 3750 psi (and an associated axial load of 110.3 ksi) and a temperature change of -480°F. Furthermore, as seen in Table 9, if the internal pressure is increased from 3750 psi to 5000 psi, the strain associated with buckling is surpassed for each fiber layup.

Table 8. Calculated Strain for a 0.015 in Liner with Varying Fiber Layup Subjected to an Internal Pressure of 3.75 ksi, an Axial Load of 110.3 ksi and an Temperature Change of ΔT=-480 °F

Fiber Layup	Thermal Strain (με)	Internal Pressure Strain (με)	Axial Strain (με)	Total Strain (με)
$[88°]_4/[17°]_2$	-2070	-2787	9186	4329
$[88°]_4/[17°]_3$	-1450	-2462	6825	2913
$[88°]_4/[17°]_2/[45°]$	-1768	-3773	8527	2986
$[88°]_4/[17°]_2/[30°]$	-1555	-3241	7560	2764

Table 9. Calculated Strain for a 0.015 in Liner with Varying Fiber Layup Subjected to an Internal Pressure of 5.0 ksi, an Axial Load of 147.1 ksi and an Temperature Change of ΔT=-480 °F

Fiber Layup	Thermal Strain (με)	Internal Pressure Strain (με)	Axial Strain (με)	Total Strain (με)
$[88°]_4/[17°]_3$	-1450	-3280	9099	4369
$[88°]_4/[17°]_2/[45°]$	-1768	-5030	11369	4571
$[88°]_4/[17°]_2/[30°]$	-1555	-4321	10081	4205

This same iterative technique was also employed for several liner thicknesses other than 0.015 in. However, in each of these instances, it was not possible to achieve

the strain necessary for buckling. The internal pressure was increased in small increments in an effort to surpass the required buckling strain value, however, for liner thicknesses greater than 0.015 in, it was found that the vessel would burst prior to achieving the required strain.

When the vessel geometry and fiber orientations that were used for the actual pressure vessel tests as described in Section 4.3 were input into the buckling program, it was found that the in order to achieve a pressure vessel strain equivalent to the that associated with the critical buckling load for the 0.040 in thick aluminum liner, the pressure vessel would have to be internally pressurized to over 8000 psi. The expected burst pressure for these vessels was 4-5 ksi, meaning that the vessel would burst long before buckling could occur. While it is encouraging that the results we observed (lack of any signs of buckling) are consistent with the results of the analytical model, it is also disappointing to realize that the designed tests were not anywhere close to producing the desired buckling effect that was under investigation. Furthermore, while the buckling tests that were performed did not come close to producing a sufficient amount of plastic deformation, in retrospect it was found that another important issue that was overlooked by HEI Engineers during the course of these buckling tests is the increase in strength that is demonstrated by the aluminum at cryogenic temperatures. As seen from Figure 33 in Appendix C, up to a 15% increase in yield strength is achieved in the aluminum, making it even more difficult to achieve the plastic deformation required in the liner.

The material properties used in the preceding analyses were based upon using IM7 Graphite Fiber. This is an intermediate modulus fiber with mechanical properties listed Appendix C.

Section 6.6 – Future Testing

It was anticipated that another set of liners could be chemically etched down to a sidewall thickness of 0.015 in and another series of buckling tests could be performed in an attempt to substantiate the results of this analysis, unfortunately, time and budget restraints did not allow this to happen.

CHAPTER 7

DISCUSSION OF RESULTS AND CONCLUSIONS

Section 7.1– Bonding Conclusions

Several key conclusions can be made from the tensile tests that were conducted. First, the tests involving the resin systems designed for use in ambient conditions clearly demonstrate that in order to maintain the bond integrity for cryogenic applications, a flexible, low modulus resin system must be used. It is believed that the poor performance of the West 105 and Epon 828 resin systems can be attributed to their brittle nature. The cryogenic environment further intensified this behavior and the thermal stresses due to the difference in the CTE were sufficient to cause failure.

Another key finding from the testing is that the samples prepared with a resin prebond achieved a significantly higher tensile strength than those without. The large disparity between the CTE of the test piece and composite laminate proved to be very problematic. The negative CTE of the graphite laminate (in the fiber direction) caused the laminate to expand as the temperature decreases, while the aluminum test fixture contracts. One reason the prebond proved to be so successful during the low temperature testing is that the thin layer of resin helped to offset the large displacement between the CTE's. Furthermore, the prebond must be sufficiently rough to create a strong mechanical bond.

Based on the limited number of tests conducted, one interesting piece of information discovered was that the neither the surface preparation or the prebond thickness had a significant effect on the cryogenic tensile strength of the samples

prepared with the HEI 535 prebond. It is believed that due to the more brittle nature of the HEI 535 at cryogenic temperatures, the surface preparation and bondline thickness have little effect on the overall performance of the test specimen. However, for the samples prepared with the more flexible AK 423 prebond, the specimens with the surface etchant used in conjunction with a thin bondline performed considerably better. One possible explanation for the superior performance of the thin prebond is the greater probability of microscopic imperfections in the thick samples, increasing the susceptibility of brittle fracture. It is recommended that further testing be conducted in order to further establish this observation.

Finally, the samples that were prepared using the grit blast and surface etchant surface preparation techniques demonstrated a failure mode where the bond between the composite and the prebond and the bond at the prebond aluminum interface would fail nearly simultaneously.

Section 7.2 – Impact Conclusions

The introduction of the energy absorbing zylon fibers with the high strength carbon fibers significantly increased the strength of the NOL ring after impact in a cryogenic environment. It was observed during the testing process that the increased toughness of the hybrid structure allows more impact energy to be absorbed before the original strength is significantly compromised.

Section 7.2.1 – Resins

Of the three resin systems investigated, HEI 535 and AK 423 performed very comparably in the impact testing. When the average breaking energy tests were

conducted for each of the different fiber configurations, the values for the HEI 535 and AK 423 samples were nearly identical, both achieving a significantly greater breaking energy than that of the Epon 862.

Although Epon 862 was not included for evaluation in the bonding tests, it is logical to conclude that as it is also a epoxy based resin system not designed for cryogenic applications, a performance similar to that of Epon 828 could be expected. Despite the fact that HEI engineers have observed that Epon 862 has an affinity for zylon fiber, it is not rational to expect that this resin system would be the best candidate for a COPV intended for use in a cryogenic application.

Alternatively, both HEI 535 and AK 423 would be considered viable candidates based upon their comparable performance in both the tensile and impact testing, although as mentioned in Section 5.4, the short pot life of AK 423 can lead to some manufacturing difficulties.

Section 7.2.2 – Fibers

Despite their high tensile strength, the all carbon impact samples behaved in a very brittle manner, with an average breaking of only 2.92 in-lbs. The predominant trend observed during the impact testing with respect to the fiber configuration was that energy absorption and plastic deformation increased as more zylon fibers were added to the composite layup.

Based upon the results of the impact tests, it would seem irrational to design a COPV with an all carbon fiber layup if there is even the slightest chance that it will be subjected to any type of impact.

The optimum fiber configuration to minimize impact damage would be placing layers of zylon on the outside of the pressure vessel, over the top of high-strength carbon fiber in a symmetric orientation. This is suggested such that the tough, energy absorbing zylon material could protect the high-strength, yet brittle carbon fibers.

Section 7.3 – Buckling Conclusions

Based on the buckling analysis of Section 6, the results show that for the given liner geometry, it would only be possible for buckling to occur in a liner that had been chemically etched down to a sidewall thickness of 0.015 in. Multiple cases were examined for the thicker liners where the amount and orientation of the composite overwrap was varied yet it was still found that the cylinder would burst prior to the occurrence of buckling. This is due largely in part to the substantial compressive strain that must be overcome due to the cryogenic environment.

Despite the fact that the experimental attempts to demonstrate liner buckling were unsuccessful, this analysis method is still considered to be very useful. One major obstacle in the experimental efforts was working with a predefined cylinder geometry that was very short.

In most real world applications, an "off-the-shelf" liner would not be used; rather one would be designed and fabricated based upon the pressure and volume requirements of the application. This is where the buckling analysis could come in very useful. It is conceived that a design engineer could employ this methodology in optimizing the liner thickness and length without having to be concerned with liner buckling.

In conclusion, as deep space exploration continues to grow on a global scale, it is anticipated that the information gathered during the course of this effort will prove beneficial for many of those who are involved in this grand undertaking.

REFERENCES

[1] Tudela, M., and Kim, R. "Impact Damage Response of Composite Materials at LOX/Cryogenic Temperatures," *AIAA*, 2157, pp. 4356-4367, 2005.

[2] Gomez-del Rio,T., Zaera, R., Barbero, E., and Navarro, C., 2005, "Damage in CFRPs due to Velocity Impact at Low Temperature," *Composite Part B: Engineering*, 34, pp. 41-50.

[3] Ohtani, K., Numata,D., Kikuchi, T., Sun, M., Takayama, K., and Togami, K., 2006, "A Study of Hypervelocity Impact on Cryogenic Materials," *International Journal of Impact Engineering*, *33*, pp. 555-565.

[4] Lopez-Puente, J., Zaera, R., Navarro, C., 2005, "The Effect of Low Temperatures on the Intermediate and High Velocity Impact Response of CFRPs," *Composites Part B: Engineering*, 33, pp. 559.

[5] Whitley, K.S., and Gates, T.S., 2001, "Tensile Properties of Polymeric Matrix Composites Subjected to Cryogenic Environments," *American Society of Composites 16th Annual Technical Conference*.

[6] Saka, K., and Harding, J., 1990, "A Simple Laminate Theory Approach to the Prediction of the Tensile Impact Strength of Woven Laminates," Oxford University Engineering Laboratory Rep 1847/90.

[7] Agarwal, Bhagwan, D., Broutman, and Lawrence, J., 1990; *Analysis and Performance of Fiber Composites*. John Wiley & Sons, Inc., Toronto.

[8] Melcher, R.J., and Johnson, W.S., 2007, "Mode I Fracture Toughness of and Adhesively Bonded Composite-Composite Joint in a Cryogenic Environment," *Composites Science and Technology*, 67 (3-4), pp. 501-506, March.

[9] Goeders, D., and Perry, J., 1991, "Adhesive Bonding Peek/IM-6 Composite for Cryogenic Applications," *36th International SAMPE Symposium and Exhibition*, pp. 348-361, April.

[10] Lawcock, G., Ye, L., Mai, Y., and Teh, C., 1997, "The Effect of Adhesive Bonding between Aluminum and Composite Prepreg on the Mechanical Properties of Carbon Fiber Reinforced Metal Laminates," *Composites Science and Technology*, 57, pp 35.

[11] Hu, X., and Huang, P.,2004, "Study on the Phase Behavior of a Toughened Epoxy Adhesive and its Bond-Strength Properties and Liquid Nitrogen Temperature," *Journal of Adhesion Science and Technology*, 18 (7), pp. 807-815.

[12] Shimoda, T., Morino, Y., Mizuntani, S., 2002 "Study of Cryogenic Mechanical Strength and Fracture Behavior of Adhesives for CFRP Tanks of Reusable Launch Vehicles," *23rd International Symposium on Space Technology and Science*, pp. 484-489.

[13] Glass, D. E., 1997, "Bonding and Sealing Evaluations for Cryogenic Tanks," *NASA Contractor Report 201734*, pp. 1-28, August.

[14] Anderson, T.L., 2004, *Fracture Mechanics – Fundamentals and Applications,* 3rd edition. CRC Publishing, New York.

[15] ASTM D3528-96, 2007, "Standard Test Method for Strength Properties of Double Lap Shear Adhesive Joints by Tension Loading," ASTM International, West Conshohocken, PA.

[16] ASTM D952-02, 2007, "Standard Test Method for Bond or Cohesive Strength of Sheet Plastics and Electrical Insulating Materials," ASTM International, West Conshohocken, PA.

[17] ASTM D2290-04, 2007 "Standard Test Method for Apparent Hoop Tensile Strength of Plastic or Reinforced Plastic Pipe by Split Disk Method," ASTM International, West Conshohocken, PA.

[18] Flugge, W., 1960, *Stresses in Shells,*Springer-Verlag, Berlin.

[19] Fronk, T. H., Folkman, S. L., and Clark, E. A., 2009, "Simple Analytical Techniques for Laminated Cylinders and Plates." *SAMPE Conference Journal , Wichita Kansas*.

[20] Herakovich, C., 1997, *Mechanics of Fibrous Composites,*Wiley, Hoboken, NJ.

APPENDICES

APPENDIX A

REPRESENTATIVE TEST MATRICES

Table 10. Double Lap Shear Test Matrix

Test No	Resin System	Temperature	Surface Finish	Bondline Thickness	Failure Load	Failure Mode
1	HEI 535	Ambient	Course (180 Grit)	Thick (0.015”)	--- lb	Bond to AL / Composite
2			Fine (100 Grit)	Thin (0.005”)	--- lb	Bond to AL / Composite
3		Cryogenic	Fine (100 Grit)	Thick (0.015”)	--- lb	Bond to AL / Composite
4			Course (180 Grit)	Thin (0.005”)	--- lb	Bond to AL / Composite
5	Urethane	Ambient	Course (180 Grit)	Thin (0.005”)	--- lb	Bond to AL / Composite
6			Fine (100 Grit)	Thick (0.015”)	--- lb	Bond to AL / Composite
7		Cryogenic	Course (180 Grit)	Thick (0.015”)	--- lb	Bond to AL / Composite
8			Fine (100 Grit)	Thin (0.005”)	--- lb	Bond to AL / Composite

Table 11. Tensile Test Matrix

Test No	Prebond Material	Surface Prep	Prebond Thickness	Failure Load (lb)	Failure Mode
1	HEI 535 / AK 423 / Epon 862 / West 105	AC 130 / Grit Blast	Thick	--- lb	AL / Prebond / Composite Interface
2				--- lb	AL / Prebond / Composite Interface
3			Thin	--- lb	AL / Prebond / Composite Interface
4				--- lb	AL / Prebond / Composite Interface
5		Sanded / As Machined	Thick	--- lb	AL / Prebond / Composite Interface
6				--- lb	AL / Prebond / Composite Interface
7			Thin	--- lb	AL / Prebond / Composite Interface
8				--- lb	AL / Prebond / Composite Interface

Table 12. COPV Liner Buckling Test Matrix

	Prebond Material / Thickness / Surface Prep				
Test No:	HEI 535 / Thick / AC 130	AK 423 / Thin / AC 130	AK 423 / Thin / Grit Blast	HEI 535 / Thin / Grit Blast	Nothing
1	Liner No: S1203				
2		Liner No: S1208			
3			Liner No: S1212		
4				Liner No: S1207	
5					Liner No: S1215

Table 13. NOL Impact / Tensile Test Matrix

Resin	Fiber	Impact	Test No.	Impact Energy	Tensile Load
HEI 535 Urethane Epon 828	All Carbon	High Impact	1	--- in lb	--- lb
			2	--- in lb	--- lb
			3	--- in lb	--- lb
		Low Energy	4	--- in lb	--- lb
			5	--- in lb	--- lb
			6	--- in lb	--- lb
		No Impact	7	--- in lb	--- lb
			8	--- in lb	--- lb
			9	--- in lb	--- lb
	2 Carbon /3 Zylon	High Energy	10	--- in lb	--- lb
			11	--- in lb	--- lb
			12	--- in lb	--- lb
		Low Energy	13	--- in lb	--- lb
			14	--- in lb	--- lb
			15	--- in lb	--- lb
		No Impact	16	--- in lb	--- lb
			17	--- in lb	--- lb
			18	--- in lb	--- lb
	3 Carbon / 2 Zylon	No Impact	19	--- in lb	--- lb
			20	--- in lb	--- lb
			21	--- in lb	--- lb
		High Energy	22	--- in lb	--- lb
			23	--- in lb	--- lb
			24	--- in lb	--- lb
		Low Energy	25	--- in lb	--- lb
			26	--- in lb	--- lb
			27	--- in lb	--- lb
	All Zylon	No Impact	28	--- in lb	--- lb
			29	--- in lb	--- lb
			30	--- in lb	--- lb
		High Energy	31	--- in lb	--- lb
			32	--- in lb	--- lb
			33	--- in lb	--- lb
		Low Energy	34	--- in lb	--- lb
			35	--- in lb	--- lb
			36	--- in lb	--- lb

APPENDIX B

TEST RESULTS

Section B1 – Double Lap Shear Test Results

Table 14. Double Lap Shear Test Results (11 June, 2007)

Test No	Resin System	Temperature	Surface Finish	Bondline Thickness	Failure Load (lbf)	Shear Stress (psi)	Failure Mode
1	HEI 535	Ambient	Course	Thick	2807.5	1452.2	Adhesive Failure
2			Fine	Thin	3251.5	1681.8	Adhesive Failure
3		Cryogenic	Fine	Thick	1123.7	581.2	Adhesive Failure
4			Course	Thin	611.5	316.3	Adhesive Failure
5	Urethane	Ambient	Course	Thin	659.1	340.9	Adhesive Failure
6			Fine	Thick	425.3	220.0	Adhesive Failure
7		Cryogenic	Course	Thick	163.4	84.5	Adhesive Failure
8			Fine	Thin	29.2	15.0	Adhesive Failure

Section B2 – Tensile Test Matrices – Already Cured Laminate

Table 15. Cryogenic Tensile Test Results (03 July, 2007)

Adhesive	Bondline Thickness	AL Finish	Test No	Failure Load (lbf)	Bond Strength (psi)	Failure Mode
Epon 862	Thick (0.015)	Abrasive	1	8.2	2.6	Bond To AL
		Abrasive	2	5.6	1.8	Bond To AL
		As Machined	3	6.4	2.0	Bond To AL
		As Machined	4	0.4	0.1	Bond To AL
	Thin (0.005)	Abrasive	5	1.9	0.6	Bond To AL
		Abrasive	6	38.6	12.3	Bond To AL
		As Machined	7	Broke Loading	N/A	Bond To AL
		As Machined	8	Broke in Cooler	N/A	Bond To AL
West 105	Thick (0.015)	Abrasive	9	Broke in Cooler	N/A	Bond To AL
		Abrasive	10	Broke in Cooler	N/A	Bond To AL
		As Machined	11	Broke in Cooler	N/A	Bond To AL
		As Machined	12	Broke in Cooler	N/A	Bond To AL
	Thin (0.005)	Abrasive	13	12.4	3.9	Bond To AL
		Abrasive	14	Broke Loading	N/A	Bond To AL
		As Machined	15	33.7	10.7	Bond To AL
		As Machined	16	33.0	10.5	Bond To AL
Urethane	Thick (0.015)	Abrasive	17	1734.4	552.1	Bond To AL
		Abrasive	18	1350.7	429.9	Bond To AL
		As Machined	19	1356.7	431.8	Bond To AL
		As Machined	20	961.1	305.9	Bond To AL
	Thin (0.005)	Abrasive	21	960.3	305.7	Bond To AL
		Abrasive	22	1444.8	459.9	Bond To AL
		As Machined	23	282.9	90.1	Bond To AL
		As Machined	24	1112.1	353.9	Bond To AL
HEI 535	Thick (0.015)	Abrasive	25	49.8	15.9	Bond To AL
		Abrasive	26	26.2	8.3	Bond To AL
		As Machined	27	10.9	3.5	Bond To AL
		As Machined	28	25.1	7.9	Bond To AL
	Thin	Abrasive	29	578.5	184.1	Bond To AL

	(0.005)	Abrasive	30	1066.7	339.5	Bond To AL
		As Machined	31	151.7	48.3	Bond To AL
		As Machined	32	19.9	6.3	Bond To AL

Table 16. Ambient Tensile Test Results (13 July, 2007)

Adhesive	Bondline Thickness	AL Finish	Test No	Failure Load (lbf)	Bond Strength (psi)	Failure Mode
Epon 862	Thick (0.015)	Abrasive	1	3106.7	988.9	Composite
		Abrasive	2	4305.0	1370.3	Composite
		As Machined	3	4235.0	1348.0	Both
		As Machined	4	3243.3	1032.4	Composite
	Thin (0.005)	Abrasive	5	3448.3	1097.6	Composite
		Abrasive	6	3730.0	1187.3	Composite
		As Machined	7	3958.3	1259.9	Composite
		As Machined	8	3736.7	1189.4	Composite
West 105	Thick (0.015)	Abrasive	9	212.0	67.5	Bond to AL
		Abrasive	10	194.1	61.8	Bond to AL
		As Machined	11	156.2	49.7	Bond to AL
		As Machined	12	69.7	22.2	Bond to AL
	Thin (0.005)	Abrasive	13	10.9	3.5	Bond to AL
		Abrasive	14	82.8	26.4	Bond to AL
		As Machined	15	14.6	4.6	Bond to AL
		As Machined	16	28.5	9.1	Bond to AL
Urethane	Thick (0.015)	Abrasive	17	823.3	262.1	Bond to AL
		Abrasive	18	708.3	225.5	Bond to AL
		As Machined	19	1193.3	379.8	Bond to AL
		As Machined	20	1293.3	411.7	Bond to AL
	Thin (0.005)	Abrasive	21	730.0	232.4	Bond to AL
		Abrasive	22	1455.0	463.1	Bond to AL
		As Machined	23	1450.0	461.6	Bond to AL
		As Machined	24	743.3	236.6	Bond to AL
HEI 535	Thick (0.015)	Abrasive	25	7233.3	2302.4	Both
		Abrasive	26	7225.0	2299.8	Both
		As Machined	27	7450.0	2371.4	Both
		As Machined	28	6145.0	1956.0	Both
	Thin (0.005)	Abrasive	29	3885.0	1236.6	Bond to AL
		Abrasive	30	6630.0	2110.4	Both
		As Machined	31	6071.6	1932.7	Both
		As Machined	32	5980.0	1903.5	Composite

Section B3 – Bonding to a Co-Cured Laminate

Table 17. Tensile Test Results (7 August, 2007)

Test No	Resin System	Prebond Thickness	Temperature	Failure Load (lbf)	Failure Mode	Bond Strength psi
1	HEI 535	Thin	Ambient	1273.2	Bond to AL	405.2
2	Urethane	Thick	Ambient	255.9	Bond to AL	81.5
3	Urethane	Thin	Cryo	402.3	Prebond to Comp	128.1
4	HEI 535	Thick	Cryo	585.3	Bond to AL	186.2
5	Urethane	Uncontrolled	Ambient	184.3	Bond to AL	58.7
6	HEI 535	Uncontrolled	Ambient	402	Bond to AL	127.9
7	HEI 535	Uncontrolled	Cryo	666.2	Bond to AL	212.1
8	Urethane	Uncontrolled	Cryo	147.6	Bond to AL	46.9
9	HEI 535	Thin	Ambient	1220	Bond to AL	388.3
10	Urethane	Thick	Ambient	231.9	Bond to AL	73.8
11	Urethane	Thin	Cryo	1977.6	Prebond to Comp	629.5
12	HEI 535	Thick	Cryo	140.5	Bond to AL	44.7
13	Urethane	Uncontrolled	Ambient	186.5	Bond to AL	59.4
14	HEI 535	Uncontrolled	Ambient	539.7	Bond to AL	171.8
15	HEI 535	Uncontrolled	Cryo	42	Bond to AL	13.4
16	Urethane	Uncontrolled	Cryo	360.8	Bond to AL	114.9

Table 18. Cryogenic Tensile Test Results (19 September, 2007)

Adhesive	Bondline Thickness	Test No	Failure Load (lbf)	Failure Mode	Bond Strength (psi)
HEI 535	No Bond	1	202.7	Bond to Al	64.5
		2	209.8	Bond to Al	66.8
		3	168.6	Bond to Al	53.7
		4	184	Bond to Al	58.6
		5	131.5	Bond to Al	41.9
		6	103.4	Bond to Al	32.9
		7	418.1	Bond to Al	133.1
		8	276.9	Bond to Al	88.1
HEI 535	Thin (0.005)	9	234.9	Bond to Al	74.8
		10	263.8	Prebond to AL	83.9
		11	197.1	Prebond to Comp	62.7
		12	198.2	Prebond to AL	63.1
	Thick (0.015)	13	116.5	Partial Failure of Both	37.1
		14	285.9	Partial Failure of Both	91.0
		15	685.7	Prebond to AL	218.3
		16	307.2	Prebond to AL	97.8

Table 19. Tensile Test Results (10 March, 2008)

Test No:	Temperature:	Prebond Material	Prebond Thickness	Failure Load (lbf)	Failure Stress (psi)	Failure Mode
1	CRYO	AK 423	Thick	450.7	143.5	Prebond to the AL
2				713	226.9	Prebond to the AL
3			Thin	1204.6	383.4	Prebond to the AL
4				381.8	121.5	Prebond to the AL
5		HEI 535	Thin	321.1	102.2	Prebond to the AL
6				965.2	307.2	Prebond to the AL
7	Ambient	AK 423	Thin	1467.6	467.2	Prebond to the AL
8				1430.9	455.5	Prebond to the AL

Table 20. Cryogenic Tensile Test Results (10 March, 2008)

Test No	Prebond Material	Surface Prep	Prebond Thickness	Failure Load (lb)	Failure Stress (psi)	Failure Mode
1	HEI 535	AC 130	Thick	198.6	63.2	Prebond to the Composite
2				120.3	38.3	Prebond to the Composite
3			Thin	330.9	105.4	Prebond to the Composite
4				258.5	82.3	Prebond to the Composite
5		Grit Blast	Thick	240.2	76.5	Prebond to the Composite
6				262.7	83.61	Prebond to the Composite
7			Thin	123.3	39.2	Prebond to the Composite
8				189.6	60.4	Prebond to the Composite
9	AK 423	AC 130	Thick	212.8	67.7	Prebond to the Composite
10				374.7	119.3	Prebond to the Composite
11			Thin	277.6	88.4	Prebond to the Composite
12				496.8	158.2	Prebond to the Composite
13		Grit Blast	Thick	406.8	129.5	Prebond to the Composite
14				397.54	126.5	Prebond to the Composite
15			Thin	215.1	68.5	Prebond to the Composite
16				747.1	237.8	Prebond to the Composite

Table 21. Cryogenic Tensile Test Results (11 Jul 2008)

Test No	Prebond Material	Surface Prep	Prebond Thickness	Failure Load (lbf)	Failure Stress (psi)	Failure Mode
1	HEI 535	AC 130	Thick	888.6	282.9	Prebond to Composite
2				1491.6	474.8	Half w/ some fiber on Pre
3			Thin	1123.3	357.6	Prebond to Composite
4				983.9	313.2	Half and Half
5		Grit Blast	Thick	1061.5	337.9	Prebond to AL w/ chunks on AL
6				1282.5	408.3	Prebond to AL
7			Thin	1110.2	353.4	Prebond to AL
8				1101.2	350.5	Prebond to AL
9	AK 423	AC 130	Thick	575.5	183.2	Prebond to Composite
10				764.4	243.3	Prebond to Composite
11			Thin	1454.5	462.9	Prebond to Composite
12				1682.3	535.5	Pre to Comp w/ fiber on Comp
13		Grit Blast	Thick	1058.9	337.0	Half and Half
14				598.4	190.5	Prebond to AL
15			Thin	850.5	270.7	Cntr Pre to AL, Out Pre to Comp
16				1163.7	370.4	Prebond to Composite

Section B4 – NOL Impact / Tensile Testing

Table 22. NOL Testing - AK 423 (21 April, 2009)

Resin	Fiber	Impact	Test No.	Width (in)	Thickness (in)	Impact Energy (in-lbs)	Tensile Load (lb)	Strength (ksi)
AK 423	All Carbon	No Impact	1	0.335	0.022	0	5875.1	398.6
			2	0.332	0.023	0	6251.9	409.4
			3	0.325	0.023	0	6365.1	425.8
		Low Energy (25%)	4	0.321	0.024	0.5	6213.4	403.3
			5	0.320	0.022	0.5	6289.0	446.7
			6	0.325	0.023	0.5	6509.4	435.4
		High Impact (75%)	7	0.323	0.023	1.5	5384.9	362.4
			8	0.325	0.023	1.5	5929.2	396.6
			9	0.325	0.023	1.5	5330.9	356.6
	2 Carbon /3 Zylon	No Impact	10	0.330	0.020	0	3936.8	298.2
			11	0.331	0.021	0	4259.8	306.4
			12	0.322	0.020	0	4187.1	325.1
		Low Energy (25%)	13	0.325	0.022	10.5	2324.5	162.6
			14	0.333	0.021	10.5	2355.6	168.4
			15	0.326	0.021	10.5	2230.5	162.9
		High Impact (75%)	16	0.322	0.020	31.1	2051.8	159.3
			17	0.325	0.023	31.1	2052.9	137.3
			18	0.327	0.019	31.1	155.9	12.5
	3 Carbon / 2 Zylon	No Impact	19	0.325	0.019	0	4857.0	393.3
			20	0.325	0.020	0	4630.7	356.2
			21	0.325	0.019	0	4693.6	380.1
		Low Energy (25%)	22	0.320	0.020	8.2	4284.5	334.7
			23	0.321	0.019	8.2	4360.6	357.5
			24	0.330	0.019	8.2	4716.5	376.1
		High Impact (75%)	25	0.330	0.019	24.6	3475.9	277.2
			26	0.326	0.020	24.6	2875.3	220.5
			27	0.326	0.020	24.6	2659.1	203.9
	All Zylon	No Impact	28	0.340	0.012	0	4939.1	605.3
			29	0.340	0.013	0	4341.8	491.2
			30	0.337	0.013	0	4641.9	529.8
		Low Energy (25%)	31	0.330	0.013	11.2	4551.3	530.5
			32	0.335	0.013	11.2	4515.3	518.4
			33	0.321	0.013	11.2	4299.1	515.1

		High Impact (75%)	34	0.330	0.012	35.5	4358.7	550.3
			35	0.351	0.013	35.5	4782.8	524.1
			36	0.32	0.013	35.5	4085.154	491.0

Table 23. NOL Testing - Epon 828 (April 23, 2009)

Resin	Fiber	Impact	Test No.	Width (in)	Thickness (in)	Impact Energy (in-lbs)	Tensile Load (lb)	Strength (ksi)
Epon 828	All Carbon	No Impact	1	0.335	0.023	0	4973.9	322.8
			2	0.332	0.023	0	5094.6	333.6
			3	0.325	0.024	0	4953.3	317.5
		Low Energy (25%)	4	0.321	0.024	0.7	5337.3	346.4
			5	0.320	0.023	0.7	5291.23	359.5
			6	0.325	0.024	0.7	4924.8	315.7
		High Impact (75%)	7	0.323	0.024	2.0	5216.3	336.5
			8	0.325	0.025	2.0	0.0	0.0
			9	0.325	0.024	2.0	0.0	0.0
	2 Carbon /3 Zylon	No Impact	10	0.330	0.020	0	4444.5	336.7
			11	0.331	0.020	0	4606.7	347.9
			12	0.322	0.020	0	4376.7	339.8
		Low Energy (25%)	13	0.325	0.020	7.6	3882.5	298.7
			14	0.333	0.020	7.6	4198.3	315.2
			15	0.326	0.021	7.6	4012.5	293.1
		High Impact (75%)	16	0.322	0.020	22.7	2324.2	180.5
			17	0.325	0.020	22.7	2317.4	178.3
			18	0.327	0.020	22.7	1944.9	148.7
	3 Carbon / 2 Zylon	No Impact	19	0.325	0.020	0	4886.2	375.9
			20	0.325	0.019	0	4559.9	369.2
			21	0.325	0.020	0	4883.6	375.7
		Low Energy (25%)	22	0.320	0.020	6.5	4094.9	319.9
			23	0.321	0.020	6.5	3968.6	309.1
			24	0.330	0.019	6.5	4029.3	321.3
		High Impact (75%)	25	0.330	0.020	19.4	3672.3	278.2
			26	0.326	0.020	19.4	3612.7	277.1
			27	0.326	0.020	19.4	2964.1	227.3
	All Zylon	No Impact	28	0.340	0.013	0	3565.8	403.4
			29	0.340	0.015	0	4241.8	415.9
			30	0.337	0.015	0	4038.7	399.5
		Low Energy (25%)	31	0.330	0.015	11.3	2748.9	277.7
			32	0.335	0.015	11.3	2765.5	275.2
			33	0.321	0.015	11.3	2674.9	277.8
		High Impact (75%)	34	0.330	0.015	34.1	2556.1	258.2
			35	0.351	0.015	34.1	2493.9	236.8
			36	0.320	0.015	34.1	2622.0	273.2

Table 24. NOL Testing - HEI 535 (April 25, 2009)

Resin	Fiber	Impact	Test No.	Width (in)	Impact Energy (in-lbs)	Tensile Load (lb)	Strength (ksi)
HEI 535	All Carbon	High Impact	1	0.320	3.0	85.1	4.9
			2	0.322	3.0	350.0	20.1
			3	0.323	3.0	366.8	21.1
		Low Energy	4	0.331	1.0	5842.8	326.9
			5	0.331	1.0	6003.9	335.9
			6	0.321	1.0	6500.0	374.9
		No Impact	7	0.327	0	5776.5	327.1
			8	0.318	0	6938.4	404.1
			9	0.317	0	5616.5	328.1
	2 Carbon /3 Zylon	High Energy	10	0.327	31.5	3688.4	281.9
			11	0.328	31.5	4177.7	318.4
			12	0.328	31.5	3846.5	293.2
		Low Energy	13	0.322	10.6	4721.0	366.5
			14	0.328	10.6	4250.0	323.9
			15	0.324	10.6	4108.0	316.9
		No Impact	16	0.325	0	4555.0	350.4
			17	0.321	0	5020.7	391.0
			18	0.321	0	5048.8	393.2
	3 Carbon / 2 Zylon	No Impact	19	0.326	0	4896.7	375.5
			20	0.331	0	5117.4	386.5
			21	0.329	0	5302.1	402.9
		High Energy	22	0.328	27.9	3667.8	279.6
			23	0.328	27.9	3822.9	291.4
			24	0.327	27.9	844.5	64.6
		Low Energy	25	0.331	9.3	5283.0	399.0
			26	0.328	9.3	5062.3	385.9
			27	0.330	9.3	4135.7	313.3
	All Zylon	No Impact	28	0.325	0	2889.9	296.4
			29	0.325	0	3031.6	310.9
			30	0.325	0	2869.3	294.3
		High Energy	31	0.321	44.6	2651.2	275.3
			32	0.320	44.6	2725.1	283.9
			33	0.325	44.6	2741.5	281.2
		Low Energy	34	0.327	14.9	2768.5	282.2
			35	0.325	14.9	2963.4	303.9
			36	0.325	14.9	2731.4	280.1

APPENDIX C

MATERIAL PROPERTIES

Section C1 – Hexcel IM7 12K Graphite Fiber

Typical Fiber Properties	U.S. Units	SI Units
Tensile Strength 6K 12K	 770 ksi 822 ksi	 5.310 MPa 5.670 MPa
Tensile Modulus (Chord 6000-1000)	40.0 Msi	276 GPa
Ultimate Elongation at Failure 6K 12K	 1.8% 1.9%	 1.8% 1.9%
Density	0.0643 lb/in^3	1.78 g/cm^3
Weight/Length 6K 12K	 12.5 x 10^{-6} lb/in 25.0 x 10^{-6} lb/in	 0.223 g/m 0.446 g/m
Approximate Yield 6K 12K	 6.674 ft/lb 3.337 ft/lb	 4.48 m/g 2.24 m/g
Tow Cross Sectional Area 6K 12K	 1.94 x 10^{-4} in^2 3.89 x 10^{-4} in^2	 0.13 mm^2 0.25 mm^2
Filament Diameter	0.203 mil	5.2 microns
Carbon Content	95.0%	95.0%
Twist	Never Twisted	Never Twisted

Taken from the Manufacturer's Website

Section C2 – Toyobo Zylon Regular AS Aramid Fiber

Type		Regular	High Modulus
		AS	HM
Filament Decitex	dtex	1.7	1.7
Density	g/cm^3	1.54	1.56
Moisture Regain (65% RH)	%	2.0	0.6
Tensile Strength	cN/dtex	37	37
	GPa	5.8	5.8
	KSI	840	840
Tensile Modulus	cN/dtex	1150	1720
	GPa	180	270
	MSI	26	39
Elongation at Break	%	3.5	2.5
Melting Temperature	°C	None	None
Decomposition Temperature in Air	°C	650	650
Coefficient of Thermal Expansion	Ppm/°C		-6
Limiting Oxygen Index		68	68
Dielectric Constant at 100kHz			3.0
Dissipation Factor			0.001

Taken from the Manufacturer's Website

Section C3 – 6061 Aluminum Properties

Properties	Metric	English
Density	2.70 g/cc	0.0975 lb/in3
Hardness Brinell	30	30
Ultimate Tensile Strength	124 MPa	18.0 ksi
Tensile Yield Strength	55.3 MPa	8.00 ksi
Elongation at Break	25.0%	25.0%
Modulus of Elasticity	68.9 GPa	10,000 ksi
Ultimate Bearing Strength	228 MPa	33,100 psi
Bearing Yield Strength	103 MPa	14,900 psi
Poissons Ratio	0.330	0.330
Shear Modulus	26.0 GPa	3770 ksi
Shear Strength	82.7 MPa	12,000 psi
Coefficient of Thermal Expansion	23.6 µm/m-°C	13.1 µin/in-°F

Taken from Matweb.com

Section C4 – 6061 T6 Aluminum Properties

Properties	Metric	English
Density	2.70 g/cc	0.0975 lb/in3
Hardness Brinell	95	95
Ultimate Tensile Strength	310 MPa	45.0 ksi
Tensile Yield Strength	276 MPa	40.0 ksi
Elongation at Break	12.0%	12.0%
Modulus of Elasticity	68.9 GPa	10,000 ksi
Ultimate Bearing Strength	607 MPa	88,000 psi
Bearing Yield Strength	386 MPa	56,000 psi
Poissons Ratio	0.330	0.330
Shear Modulus	26.0 GPa	3770 ksi
Shear Strength	207 MPa	30000 psi
Coefficient of Thermal Expansion	23.6 µm/m-°C	13.1 µin/in-°F

Taken from Matweb.com

Section C5– 6061 T6 Aluminum Cryogenic Properties

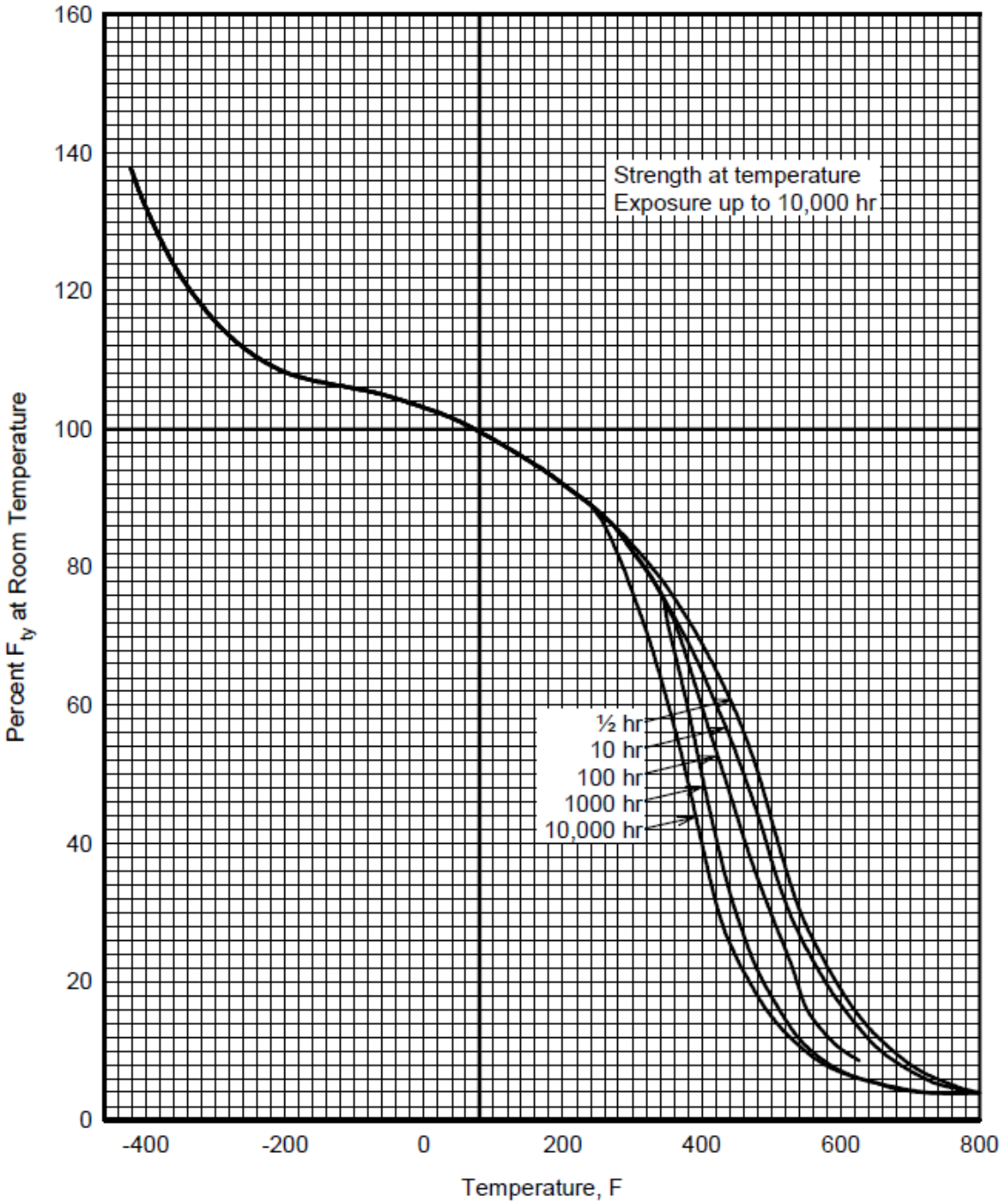

Figure 33. Effect of Temperature of the Tensile Yield Strength of 6061 T6 Aluminum Allow (Taken from MIL Handbook).

APPENDIX D

LAMINATED TUBE COMPUTER PROGRAM

```
!*************************************************************************
!
!  PURPOSE:  Calculate Stresses or Strains For a Laminated Composite Tube
!
!*************************************************************************
!  Modules
!
    Module Var
     implicit none
!
!     Variables
!
    type::lamina
            integer :: mat_type
            real (kind=kind(0.d0)):: thick
            real (kind=kind(0.d0)):: theta
    end type lamina

!  Variable Definition

            integer :: i,j,k,l,n, Pflag, Tflag,  nl, nm, nrank, Smear_Flag, L_Flag
            integer, allocatable, dimension (:) :: TIflag
            integer, parameter :: MaxLam=20
            character (len=70) :: title
    real (kind=kind(0.d0)) :: pi,sn, cs, sn2, cs2, sn4, cs4, Pin, Pout,h,Ri,Ro
    real (kind=kind(0.d0)) ::  Num1, Num2, Num3, Num4, Num5, Num6
    real (kind=kind(0.d0)) :: epsx, Px, T, gammaxt
    real (kind=kind(0.d0)) :: Den, Den1, Den2, Den3, deltaT, wri, TT
    real (kind=kind(0.d0)) :: TItest, A1, A2
            real (kind=kind(0.d0)), allocatable, dimension(:,:) :: C
            real (kind=kind(0.d0)), allocatable, dimension(:,:,:) :: CB
            real (kind=kind(0.d0)), allocatable, dimension(:,:) :: alpha
            real (kind=kind(0.d0)), allocatable, dimension(:) :: thetar, Lamda, Omega, Psi, Sigmahat, Gamma,
con1, con3, con6
            real (kind=kind(0.d0)), allocatable, dimension (:):: x, b, ELF, R, rho
    real (kind=kind(0.d0)), allocatable, dimension(:,:) :: a, KM
    type (lamina), allocatable, dimension(:) :: lam
     real (kind=kind(0.d0)), allocatable, dimension(:,:) :: epsr, epst, gamxt
            real (kind=kind(0.d0)), allocatable, dimension(:,:) :: sigx, sigt, sigr, tauxt
            real (kind=kind(0.d0)) :: CBalpha6
            real (kind=kind(0.d0)) :: Area, alphabarx, alphabarr, Nubarxt
            real (kind=kind(0.d0)) :: zetaPG, zetaTE, zetaPi, zetaDELT
            real (kind=kind(0.d0)) :: Ebarx, Gbarxt
           End module var

    Module PLib
```

```
    implicit none
            integer, parameter :: max_mats=30
            integer, dimension(max_mats) :: mat_id
            type :: materials
     character (len=32) :: description
     real (kind=kind(0.d0)) :: e1
              real (kind=kind(0.d0)) :: e2
              real (kind=kind(0.d0)) :: e3
              real (kind=kind(0.d0)) :: g12
              real (kind=kind(0.d0)) :: g13
              real (kind=kind(0.d0)) :: g23
              real (kind=kind(0.d0)) :: pr12
              real (kind=kind(0.d0)) :: pr21
              real (kind=kind(0.d0)) :: pr23
              real (kind=kind(0.d0)) :: pr32
              real (kind=kind(0.d0)) :: pr13
              real (kind=kind(0.d0)) :: pr31
              real (kind=kind(0.d0)) :: alpha1
              real (kind=kind(0.d0)) :: alpha2
            end type materials
            type (materials), dimension(max_mats) :: mat
            END MODULE PLib
!
!
!
            program LamTube
            use var
            USE PLib
            implicit none
!
!            Body of LamTube
!
    open(unit=7,file='LamTube.in',status='old')
    open(unit=8,file='LamTube.out')
            pi=acos(-1.d0)

            CALL INPUT
            CALL KMATRIX
!
!
!
    IF(L_Flag.ne.0)THEN
             CALL LOADS
     CALL SYMSOL
             If(Pflag.eq.1)then
      epsx=x(2*nl+1)
     ELSE
              Px=x(2*nl+1)
     end if
             If(Tflag.eq.1)then
      gammaxt=x(2*nl+2)
```

```
      else
               T=x(2*nl+2)
              end if
              wri=x(1)*r(0)**Lamda(1)+x(2)*r(0)**(-Lamda(1))+epsx*Gamma(1)*r(0)&
               +Omega(1)*gammaxt*r(0)**2.d0+Psi(1)*r(0)*deltaT
              CALL EPSSIG
              CALL OUTPUT
     END IF
            IF (Smear_Flag.ne.0)THEN
             CALL SMEAR
     END IF
            END
!
!
!================================================================================
!
!   SUBROUTINES
!
!================================================================================
            SUBROUTINE INPUT
            USE VAR
            USE PLib
            IMPLICIT NONE
            read(7,'(a70)')title
            read(7,*)nl,nm
            READ(7,*)(mat_id(i),i=1,nm)
!
!   Allocate Matrices
!

            nrank=2*nl+2
            if(nl.gt.MaxLam)nl=MaxLam
     Allocate (lam(nl))
            Allocate (thetar(nl))
            Allocate (alpha(nl,6))
            Allocate (x(2*nl+2))
            Allocate (b(2*nl+2))
            Allocate (elf(2*nl+2))
            Allocate (Rho(2*nl+2))
            Allocate (a(2*nl+2,2*nl+2))
            Allocate (KM(2*nl+2,2*nl+2))
            Allocate (C(nm,9))
            Allocate (CB(nl,6,6))
            Allocate (r(0:nl))
            Allocate (TIflag(nl))
            Allocate (Psi(nl))
            Allocate (Omega(nl))
            Allocate (Lamda(nl))
            Allocate (Sigmahat(nl))
            Allocate (Gamma(nl))
            Allocate (con1(nl))
```

```
            Allocate (con3(nl))
            Allocate (con6(nl))
            Allocate (epsr(nl,2),epst(nl,2),gamxt(nl,2))
            Allocate (sigx(nl,2),sigt(nl,2),sigr(nl,2),tauxt(nl,2))
!
!
!
    DO i=1,nm
     CALL PropLib(i)
    END DO
!
!
!
    alpha=0.d0
    tt=0.d0
            do i=1,nl
     read(7,*)lam(i)%mat_type,lam(i)%thick,lam(i)%theta
             thetar(i)=lam(i)%theta*acos(-1.d0)/180.d0
     tt=tt+lam(i)%thick
    end do
            do i=1,nl
             j=lam(i)%mat_type
             WRITE(6,*)i,j
     alpha(i,1)=cos(thetar(i))**2*mat(j)%alpha1+sin(thetar(i))**2*mat(j)%alpha2
     alpha(i,2)=sin(thetar(i))**2*mat(j)%alpha1+cos(thetar(i))**2*mat(j)%alpha2
     alpha(i,3)=mat(j)%alpha2
     alpha(i,6)=2.d0*cos(thetar(i))*sin(thetar(i))*(mat(j)%alpha1-mat(j)%alpha2)
            end do

            CALL MATPROPS
            read(7,*)Ri
            r(0)=Ri
            do k=1,nl
             r(k)=r(k-1)+lam(k)%thick
    end do
            READ(7,*)L_Flag, Smear_Flag
!
!   L_flag = 1  Input Loads & Delta T
!   L_flag = 0  No Load Calculations
!   Smear_flag = 1 Calculate Smeared Properties
!   Smear_flag = 0 Do Not Calculate Smeared Properties
!
            IF(L_Flag.ne.0)THEN
            read(7,*)deltaT
!
!   Input Loads or Strains
!
!   Pflag = 1 = Input Px
!   Pflag = 0 = Input epsilonx
!   Tflag = 1 = Input T
!   Tflag = 0 = Input gammaxt
```

```
!
    Px=0.d0
            epsx=0.d0
            T=0.d0
            gammaxt=0.d0
            read(7,*)Pflag
            select case (Pflag)
    case(1)
     read(7,*)Px
    case(0)
     read(7,*)epsx
            end select
            read(7,*)Tflag
            select case (Tflag)
    case(1)
     read(7,*)T
    case(0)
     read(7,*)gammaxt
    end select
    read(7,*)Pin,Pout
            END IF
            close (7)
    END SUBROUTINE
!
!    Properties
!
    SUBROUTINE PropLib(i)
            USE PLib
            IMPLICIT NONE
            integer :: i
    SELECT CASE (mat_id(i))
            CASE(1)
!
!    Aluminum (1) Eng
!
     mat(i)%description='Aluminum Eng'
     mat(i)%E1=11.d06
             mat(i)%E2=11.d06
     mat(i)%pr12=0.33d0
     mat(i)%pr23=0.33d0
             mat(i)%g12=mat(i)%E1/(2.d0*(1.d0+mat(i)%pr12))
     mat(i)%alpha1=13.11d-06
             mat(i)%alpha2=13.11d-06
    CASE(11)
!
!    Aluminum (11) SI
!
     mat(i)%description='Aluminum Eng'
     mat(i)%E1=69.d09
             mat(i)%E2=69.d09
     mat(i)%pr12=0.33d0
```

```
      mat(i)%pr23=0.33d0
              mat(i)%g12=mat(i)%E1/(2.d0*(1.d0+mat(i)%pr12))
      mat(i)%alpha1=23.4d-06
              mat(i)%alpha2=23.4d-06
     CASE(4)
!
!     Hyer Graphite (4) SI
!
      mat(i)%description='Hyer Graphite SI'
      mat(i)%E1=155.d09
              mat(i)%E2=12.0D09
      mat(i)%pr12=0.248d0
      mat(i)%pr23=0.458d0
              mat(i)%g12=4.4d09
      mat(i)%alpha1=-0.018d-06
              mat(i)%alpha2=24.3d-06
     CASE(15)
!
!     T300/5208 (15) Eng
!
       mat(i)%description='T300/5208 ENG'
       mat(i)%E1=19.2d06
               mat(i)%E2=1.56d06
       mat(i)%pr12=0.24d0
       mat(i)%pr23=0.59d0
               mat(i)%g12=0.82d06
       mat(i)%alpha1=-.43d-06
               mat(i)%alpha2=13.6d-06
     END SELECT

             mat(i)%pr21=(mat(i)%pr12*mat(i)%E2)/mat(i)%E1
     mat(i)%G23=mat(i)%E2/(2.d0*(1.d0+mat(i)%pr23))
     mat(i)%E3=mat(i)%E2
             mat(i)%pr32=mat(i)%pr23
     mat(i)%pr13=mat(i)%pr12
             mat(i)%pr31=mat(i)%pr21
     mat(i)%G13=mat(i)%G12
!
!
!
     RETURN
             END
!
!    STIFFNESS AND COMPLIANCE MATRICES
!
     SUBROUTINE MATPROPS
             Use var
             USE PLib
             Implicit None
     do i=1,nm
      DEN=(1.d0-2.d0*mat(i)%pr12*mat(i)%pr21-mat(i)%pr23*mat(i)%pr32-2.d0*mat(i)%pr21*&
```

```
            mat(i)%pr32*mat(i)%pr13)/(mat(i)%E1*mat(i)%E2*mat(i)%E3)
            DEN1=mat(i)%E2*mat(i)%E3*DEN
            DEN2=mat(i)%E1*mat(i)%E3*DEN
            DEN3=mat(i)%E1*mat(i)%E2*DEN
            Num1=1.d0-mat(i)%pr23*mat(i)%pr32
            Num2=mat(i)%pr21+mat(i)%pr23*mat(i)%pr31
            Num3=mat(i)%pr31+mat(i)%pr21*mat(i)%pr32
     Num4=1.d0-mat(i)%pr13*mat(i)%pr31
            Num5=mat(i)%pr32+mat(i)%pr12*mat(i)%pr31
     Num6=1.d0-mat(i)%pr12*mat(i)%pr21
            C(i,1)=Num1/Den1
            C(i,2)=Num2/Den1
            C(i,3)=Num3/Den1
            C(i,4)=Num4/Den2
            C(i,5)=Num5/Den2
            C(i,6)=Num6/Den3
            C(i,7)=mat(i)%G23
            C(i,8)=mat(i)%G13
            C(i,9)=mat(i)%G12
    end do
    CB=0.d0
    do k=1,nl
     cs=cos(thetar(k))
            sn=sin(thetar(k))
            i=lam(k)%mat_type
     cs4=cs**4
     sn4=sn**4
            cs2=cs**2
            sn2=sn**2
            CB(K,1,1)=cs4*C(i,1)+2.d0*cs2*sn2*(C(i,2)+2.d0*C(i,9))+sn4*C(i,4)
            CB(K,1,2)=cs2*sn2*(C(i,1)+C(i,4)-4.d0*C(i,9))+(sn4+cs4)*C(i,2)
            CB(K,1,3)=cs2*C(i,3)+sn2*C(i,5)
            CB(K,1,6)=sn*cs*(cs2*(C(i,1)-C(i,2)-2.d0*C(i,9))+sn2*(C(i,2)-C(i,4)+2.d0*C(i,9)))
            CB(K,2,2)=sn4*C(i,1)+2.d0*cs2*sn2*(C(i,2)+2.d0*C(i,9))+cs4*C(i,4)
     CB(K,2,3)=sn2*C(i,3)+cs2*C(i,5)
            CB(K,2,6)=sn*cs*(sn2*(C(i,1)-C(i,2)-2.d0*C(i,9))+cs2*(C(i,2)-C(i,4)+2.d0*C(i,9)))
            CB(K,3,3)=C(i,6)
            CB(K,3,6)=cs*sn*(C(i,3)-C(i,5))
            CB(K,4,4)=cs2*C(i,7)+sn2*C(i,8)
            CB(K,4,5)=sn*cs*(C(i,8)-C(i,7))
            CB(K,5,5)=sn2*C(i,7)+cs2*C(i,8)
            CB(K,6,6)=sn2*cs2*(C(i,1)-2.d0*C(i,2)+C(i,4))+C(i,9)*(sn2-cs2)**2
     DO i=1,5
      DO j=i+1,6
              CB(k,j,i)=CB(k,i,j)
      end do
     end do
          end do
!
!   Calculate lamina constants
!
```

```
    Do k=1,nl
            Lamda(k)=sqrt(CB(K,2,2)/CB(K,3,3))
            TItest=dabs(CB(K,3,3)-CB(K,2,2))
     If(TItest.lt.1.0D-08)then
            TIFlag(k)=1
            Gamma(k)=0.d0
            Omega(k)=0.d0
            Sigmahat(k)=0.d0
            Psi(k)=0.d0
     else
            TIFlag(k)=0
            Gamma(k)=(CB(K,1,2)-CB(K,1,3))/(CB(K,3,3)-CB(K,2,2))
      Omega(k)=(CB(K,2,6)-2.d0*CB(K,3,6))/(4.d0*CB(K,3,3)-CB(K,2,2))
            Sigmahat(k)=0.d0
            do i=1,6
             Sigmahat(k)=Sigmahat(k)+(CB(K,i,3)-CB(K,i,2))*alpha(k,i)
            end do
            Psi(k)=Sigmahat(k)/(CB(K,3,3)-CB(K,2,2))
     End IF
    end do
            RETURN
            END
!.....................................................................
!
!
!  Assemble Coefficient Matrix
!
!
    SUBROUTINE KMATRIX
            USE var
            implicit none
            KM=0.d0
!
!   Find Preliminary KM Matrix and Vector ELF
!
!
!           Row 1
            KM(1,1)=(CB(1,2,3)+Lamda(1)*CB(1,3,3))*ri**(Lamda(1)-1.d0)
    KM(1,2)=(CB(1,2,3)-Lamda(1)*CB(1,3,3))*ri**(-Lamda(1)-1.d0)
    KM(1,2*nl+1)=CB(1,1,3)+(CB(1,2,3)+CB(1,3,3))*Gamma(1)
            KM(1,2*nl+2)=ri*((CB(1,2,3)+2.d0*CB(1,3,3))*Omega(1)+CB(1,3,6))
!    Even Rows
    do k=1,nl-1
     KM(2*k,2*k-1)=r(k)**Lamda(k)
     KM(2*k,2*k)=r(k)**(-Lamda(k))
            KM(2*k,2*k+1)=-r(k)**Lamda(k+1)
            KM(2*k,2*k+2)=-r(k)**(-Lamda(k+1))
            KM(2*k,2*nl+1)=(Gamma(k)-Gamma(k+1))*r(k)
            KM(2*k,2*nl+2)=(Omega(k)-Omega(k+1))*r(k)**2
    end do
```

```
!   Odd Rows
    do k=1,nl-1
     KM(2*k+1,2*k-1)=(CB(k,2,3)+Lamda(k)*CB(k,3,3))*r(k)**(Lamda(k)-1)
     KM(2*k+1,2*k)=(CB(k,2,3)-Lamda(k)*CB(k,3,3))*r(k)**(-Lamda(k)-1)
            KM(2*k+1,2*k+1)=-(CB(k+1,2,3)+Lamda(k+1)*CB(k+1,3,3))*r(k)**(Lamda(k+1)-1)
            KM(2*k+1,2*k+2)=-(CB(k+1,2,3)-Lamda(k+1)*CB(k+1,3,3))*r(k)**(-Lamda(k+1)-1)
            KM(2*k+1,2*nl+1)=CB(k,1,3)+Gamma(k)*(CB(k,2,3)+CB(k,3,3))&
                    -(CB(k+1,1,3)+Gamma(k+1)*(CB(k+1,2,3)+CB(k+1,3,3)))
            KM(2*k+1,2*nl+2)=((CB(k,2,3)+2.d0*CB(k,3,3))*Omega(k)+CB(k,3,6)&
                   -((CB(k+1,2,3)+2.d0*CB(k+1,3,3))*Omega(k+1)+CB(k+1,3,6)))*r(k)
    end do
!   2N Equation
    KM(2*nl,2*nl-1)=(CB(nl,2,3)+Lamda(nl)*CB(nl,3,3))*r(nl)**(Lamda(nl)-1.d0)
    KM(2*nl,2*nl)=(CB(nl,2,3)-Lamda(nl)*CB(nl,3,3))*r(nl)**(-Lamda(nl)-1.d0)
           KM(2*nl,2*nl+1)=CB(nl,1,3)+Gamma(nl)*(CB(nl,2,3)+CB(nl,3,3))
           KM(2*nl,2*nl+2)=((CB(nl,2,3)+2.d0*CB(nl,3,3))*Omega(nl)+CB(nl,3,6))*r(nl)
!   2N+1 Equation
    do k=1,nl
     KM(2*nl+1,2*k-1)=2.d0*pi*(CB(k,1,2)+Lamda(k)*CB(k,1,3))&
                        *(r(k)**(lamda(k)+1.d0)-r(k-1)**(lamda(k)+1.d0))/(Lamda(k)+1.d0)
     IF(TIFlag(k).eq.1)then
              KM(2*nl+1,2*k)=0.d0
             else
      KM(2*nl+1,2*k)=2.d0*pi*(CB(k,1,2)-Lamda(k)*CB(k,1,3))&
                        *(r(k)**(-lamda(k)+1.d0)-r(k-1)**(-lamda(k)+1.d0))/(-Lamda(k)+1.d0)
     END IF
     KM(2*nl+1,2*nl+1)=2.d0*pi*(CB(k,1,1)+Gamma(k)*(CB(k,1,3)+CB(k,1,2)))&
                        *(r(k)**2.d0-r(k-1)**2.d0)/2.d0+KM(2*nl+1,2*nl+1)
     KM(2*nl+1,2*nl+2)=2.d0*pi*((CB(k,1,2)+2.d0*CB(k,1,3))*Omega(k)+CB(k,1,6))&
                        *(r(k)**3.d0-r(k-1)**3.d0)/3.d0+KM(2*nl+1,2*nl+2)
            end do

!   2N+2 Equation
    do k=1,nl
             KM(2*nl+2,2*k-1)=2.d0*pi*(CB(k,2,6)+Lamda(k)*CB(k,3,6))&
                        *(r(k)**(Lamda(k)+2.d0)-r(k-1)**(Lamda(k)+2.d0))/(Lamda(k)+2.d0)
     KM(2*nl+2,2*k)=2.d0*pi*(CB(k,2,6)-Lamda(k)*CB(k,3,6))&
                        *(r(k)**(-Lamda(k)+2.d0)-r(k-1)**(-Lamda(k)+2.d0))/(-Lamda(k)+2.d0)
     KM(2*nl+2,2*nl+1)= 2.d0*pi*(CB(k,1,6)+(CB(k,2,6)+CB(k,3,6))*Gamma(k))&
                        *(r(k)**3.d0-r(k-1)**3.d0)/3.d0+KM(2*nl+2,2*nl+1)
     KM(2*nl+2,2*nl+2)= 2.d0*pi*(CB(k,6,6)+(CB(k,2,6)+2.d0*CB(k,3,6))*Omega(k))&
                        *(r(k)**4.d0-r(k-1)**4.d0)/4.d0+KM(2*nl+2,2*nl+2)
    end do
            Con1=0.d0
            Con3=0.d0
            Con6=0.d0
            do k=1,nl
             DO i=1,6
              con1(k)=CB(k,i,1)*alpha(k,i)+con1(k)
              con3(k)=CB(k,i,3)*alpha(k,i)+con3(k)
              con6(k)=CB(k,i,6)*alpha(k,i)+con6(k)
```

```
      end do
     end do
!
!    End Forces
!
     Rho=0.d0
            Rho(1)=((CB(1,2,3)+CB(1,3,3))*Psi(1)-con3(1))
            Do k=1,nl-1
             Rho(2*k)=(Psi(k)-Psi(k+1))*r(k)
             Rho(2*k+1)=((CB(k,2,3)+CB(k,3,3))*Psi(k)-con3(k))&
                   -((CB(k+1,2,3)+CB(k+1,3,3))*Psi(k+1)-con3(k+1))
     End Do
            Rho(2*nl)=((CB(nl,2,3)+CB(nl,3,3))*Psi(nl)-con3(nl))
            Do k=1,nl
             Rho(2*nl+1)=((CB(k,1,2)+CB(k,1,3))*Psi(k)-con1(k))*&
                    pi*(r(k)**2-r(k-1)**2)+Rho(2*nl+1)
             Rho(2*nl+2)=((CB(k,2,6)+CB(k,3,6))*Psi(k)-con6(k))*&
                     2.d0*pi*(r(k)**3-r(k-1)**3)/3.d0+Rho(2*nl+2)
     End Do
            RETURN
            END
!
!   Apply Loads or Strains and/or DELTA T
!
     SUBROUTINE LOADS
            USE var
            implicit none
!
!    Apply delta T and construct Force vector
!
            do i=1,2*nl+2
      elf(i)=-rho(i)*deltaT
            end do
            ELF(1)=elf(1)-Pin
     ELF(2*nl)=elf(2*nl)-Pout
     ELF(2*nl+1)=elf(2*nl+1)+Px
     ELF(2*nl+2)=elf(2*nl+2)+T
!
!  If Loads are given instead of strains the KM matrix and elf vector are updated
!
     IF(Pflag.eq.0)then
      do i=1,2*nl+2
       ELF(i)=ELF(i)-KM(i,2*nl+1)*epsx
       KM(i,2*nl+1)=0.d0
      end do
             KM(2*nl+1,2*nl+1)=-1.d0
     END IF

            IF(Tflag.eq.0)then
      do i=1,2*nl+2
       ELF(i)=ELF(i)-KM(i,2*nl+2)*gammaxt
```

```
      KM(i,2*nl+2)=0.d0
     end do
              KM(2*nl+2,2*nl+2)=-1.d0
     END IF
!
!
!
              a=Km
              b=Elf
              RETURN
              END
!
!.....
!
!
!   Solve System of Equations
!
!
              SUBROUTINE SYMSOL
              use var
              implicit none
              integer :: ii, jj, i1
!             integer :: nrank
              integer :: mcol, icol
              integer, dimension(nrank) :: id
     real (kind=kind(0.d0)) :: amax
!
!    SCALING
!
              do i=1,nrank
               amax=dabs(a(i,1))
               do j=2,nrank
      if(dabs(a(i,j)).gt.amax)amax=DABS(a(i,j))
     end do
             DO j=1,nrank
     a(i,j)=a(i,j)/amax
    end do
    b(i)=b(i)/amax
   end do
!
!
!
             do i=1,nrank
     id(i)=i
    end do
!
!    PIVOTING
!
            mcol=nrank-1
            do j=1,mcol
             amax=a(id(j),j)
```

```
            icol=id(j)
            do i=j+1,nrank
             if(dabs(a(id(i),j)).GT.dabs(amax))then
              amax=a(id(i),j)
              id(j)=id(i)
              id(i)=icol
              icol=id(j)
             end if
    end do
!
!     ELIMINATION
!
            i1=id(j)
            do  i=j+1,nrank
             ii=id(i)
             b(ii)=b(ii)-b(i1)*a(ii,j)/a(i1,j)
             do  jj=j+1,nrank
     a(ii,jj)=a(ii,jj)-a(ii,j)*a(i1,jj)/a(i1,j)
    end do
           end do
   end do
!
!    BACK SUBSTITUTION
!
           x(nrank)=b(id(nrank))/a(id(nrank),nrank)
           DO i=nrank-1,1,-1
            ii=id(i)
            x(i)=b(ii)/a(ii,i)
            DO j=i+1,nrank
    x(i)=x(i)-(a(ii,j)*x(j))/a(ii,i)
    end do
   end do
           RETURN
           END
!.....................................................................
!
!
!  Find the Strains & Stresses
!
!
    SUBROUTINE EPSSIG
            USE Var
            Implicit NONE
!
!     STRAINS
!
    epsr=0.d0
            epst=0.d0
            gamxt=0.d0
            do k=1,nl
              A1=x(2*k-1)
```

```
                A2=x(2*k)
     epsr(k,1)=lamda(k)*A1*r(k-1)**(lamda(k)-1)-lamda(k)*A2*r(k-1)**(-lamda(k)-1)&
                +Gamma(k)*epsx+2.d0*Omega(k)*gammaxt*r(k-1)+Psi(k)*deltaT
     epsr(k,2)=lamda(k)*A1*r(k)**(lamda(k)-1)-lamda(k)*A2*r(k)**(-lamda(k)-1)&
                +Gamma(k)*epsx+2.d0*Omega(k)*gammaxt*r(k)+Psi(k)*deltaT
     epst(k,1)=A1*r(k-1)**(lamda(k)-1)+A2*r(k-1)**(-lamda(k)-1)&
                +Gamma(k)*epsx+Omega(k)*gammaxt*r(k-1)+Psi(k)*deltaT
     epst(k,2)=A1*r(k)**(lamda(k)-1)+A2*r(k)**(-lamda(k)-1)&
                +Gamma(k)*epsx+Omega(k)*gammaxt*r(k)+Psi(k)*deltaT
     gamxt(k,1)=gammaxt*r(k-1)
                gamxt(k,2)=gammaxt*r(k)
    end do
!
!   STRESSES
!
     sigx=0.d0
          sigt=0.d0
          sigr=0.d0
          tauxt=0.d0
          DO k=1,nl
           sigx(k,1)=(epsx-alpha(k,1)*deltaT)*CB(k,1,1)+&
                (epst(k,1)-alpha(k,2)*deltaT)*CB(k,1,2)+&
                                (epsr(k,1)-alpha(k,3)*deltaT)*CB(k,1,3)+&
          (gamxt(k,1)-alpha(k,6)*deltaT)*CB(k,1,6)
     sigx(k,2)=(epsx-alpha(k,1)*deltaT)*CB(k,1,1)+&
                (epst(k,2)-alpha(k,2)*deltaT)*CB(k,1,2)+&
                                (epsr(k,2)-alpha(k,3)*deltaT)*CB(k,1,3)+&
          (gamxt(k,2)-alpha(k,6)*deltaT)*CB(k,1,6)
            sigt(k,1)=(epsx-alpha(k,1)*deltaT)*CB(k,1,2)+&
                (epst(k,1)-alpha(k,2)*deltaT)*CB(k,2,2)+&
                                (epsr(k,1)-alpha(k,3)*deltaT)*CB(k,2,3)+&
          (gamxt(k,1)-alpha(k,6)*deltaT)*CB(k,2,6)
     sigt(k,2)=(epsx-alpha(k,1)*deltaT)*CB(k,1,2)+&
                (epst(k,2)-alpha(k,2)*deltaT)*CB(k,2,2)+&
                                (epsr(k,2)-alpha(k,3)*deltaT)*CB(k,2,3)+&
          (gamxt(k,2)-alpha(k,6)*deltaT)*CB(k,2,6)
            sigr(k,1)=(epsx-alpha(k,1)*deltaT)*CB(k,1,3)+&
                (epst(k,1)-alpha(k,2)*deltaT)*CB(k,3,2)+&
                                (epsr(k,1)-alpha(k,3)*deltaT)*CB(k,3,3)+&
          (gamxt(k,1)-alpha(k,6)*deltaT)*CB(k,3,6)
     sigr(k,2)=(epsx-alpha(k,1)*deltaT)*CB(k,1,3)+&
                (epst(k,2)-alpha(k,2)*deltaT)*CB(k,3,2)+&
                                (epsr(k,2)-alpha(k,3)*deltaT)*CB(k,3,3)+&
          (gamxt(k,2)-alpha(k,6)*deltaT)*CB(k,3,6)
          CBalpha6=0.d0
                                DO i=1,6
                                 CBalpha6=CBalpha6+CB(k,i,6)*alpha(k,i)
          END DO
            tauxt(k,1)=epsx*(CB(k,1,6)+(CB(k,2,6)+CB(k,3,6))*Gamma(k))+&
                 gammaxt*(CB(k,6,6)+(CB(k,2,6)+2.d0*CB(k,3,6))*Omega(k))*r(k-1)+&
           ((CB(k,2,6)+CB(k,3,6))*Psi(k)-CBalpha6)*deltaT+&
```

```
          (CB(k,2,6)+CB(k,3,6)*lamda(k))*A1*r(k-1)**(lamda(k)-1.d0)+&
                                    (CB(k,2,6)-lamda(k)*CB(k,3,6))*A2*r(k-1)**(-lamda(k)-1.d0)
            tauxt(k,2)=epsx*(CB(k,1,6)+(CB(k,2,6)+CB(k,3,6))*Gamma(k))+&
                  gammaxt*(CB(k,6,6)+(CB(k,2,6)+2.d0*CB(k,3,6))*Omega(k))*r(k)+&
          ((CB(k,2,6)+CB(k,3,6))*Psi(k)-CBalpha6)*deltaT+&
          (CB(k,2,6)+CB(k,3,6)*lamda(k))*A1*r(k)**(lamda(k)-1.d0)+&
                                    (CB(k,2,6)-lamda(k)*CB(k,3,6))*A2*r(k)**(-lamda(k)-1.d0)
    END DO
    return
          END
!-------------------------------------------------------------------------------
!
!    Find Laminated Tube Smeared Properties
!
!
    SUBROUTINE SMEAR
    USE var
          IMPLICIT NONE
          real (kind=kind(0.d0)) :: Jo
!
!    SMEARED PROPERTIES
!
     Area=pi*(r(nl)**2-Ri**2)
                  Jo=0.5d0*pi*(r(nl)**4-Ri**4)
                  Pflag=1
                  Tflag=1
                  Pin=0.d0
                  Pout=0.d0
!
!     CASE A  Px.ne.0
!
                  Px=1.d0
                  T=0.d0
     deltaT=0.d0
     CALL LOADS
                  CALL SYMSOL
                  epsx=x(2*nl+1)
                  gammaxt=x(2*nl+2)
                  wri=x(1)*r(0)**Lamda(1)+x(2)*r(0)**(-Lamda(1))+epsx*Gamma(1)*r(0)&
              +Omega(1)*gammaxt*r(0)**2.d0+Psi(1)*r(0)*deltaT
     Ebarx=Px/(epsx*Area)
                  WRITE(6,*)'eps=',epsx,'   gamma=',gammaxt
                  zetaPG=gammaxt*Ri/epsx !shear / axial eleongation due to AXIAL Load, Px
     Nubarxt=-wri/(epsx*Ri)
!
!     CASE B Tx.ne.0
!
                  Px=0.d0
                  T=100.d0
     deltaT=0.d0
                  CALL LOADS
```

```
                    CALL SYMSOL
                    epsx=x(2*nl+1)
                    gammaxt=x(2*nl+2)
                    wri=x(1)*r(0)**Lamda(1)+x(2)*r(0)**(-Lamda(1))+epsx*Gamma(1)*r(0)&
               +Omega(1)*gammaxt*r(0)**2.d0+Psi(1)*r(0)*deltaT

                    Gbarxt=T/(gammaxt*Jo)
                    zetaTE=epsx/(gammaxt*Ri) !axial eleongation / shear due to Torque
!
!     CASE C  delta T .ne. 0
!
                    Px=0.d0
                    T=0.d0
     deltaT=100.d0
     CALL LOADS
                    CALL SYMSOL
                    epsx=x(2*nl+1)
                    gammaxt=x(2*nl+2)
                    wri=x(1)*r(0)**Lamda(1)+x(2)*r(0)**(-Lamda(1))+epsx*Gamma(1)*r(0)&
               +Omega(1)*gammaxt*r(0)**2.d0+Psi(1)*r(0)*deltaT
                    alphabarx=epsx/deltaT
     alphabarr=wri/(Ri*deltaT)
                    zetaDELT=gammaxt*Ri/epsx !Shear / axial eleongation due to a delta T
!
!                   CASE D Pi .ne. 0
!
     Px=0.d0
                    T=0.d0
                    deltaT=0.d0
                    Pin=10.d0
     CALL LOADS
                    CALL SYMSOL
                    epsx=x(2*nl+1)
                    gammaxt=x(2*nl+2)
                    wri=x(1)*r(0)**Lamda(1)+x(2)*r(0)**(-Lamda(1))+epsx*Gamma(1)*r(0)&
               +Omega(1)*gammaxt*r(0)**2.d0+Psi(1)*r(0)*deltaT
     zetaPi=gammaxt*Ri/epsx !Shear / axial eleongation due to a Internal Pressure, Pi
!
!
!
          WRITE(8,*)
          WRITE(8,*)
          WRITE(8,*)'SMEARED PROPERTIES'
          WRITE(8,*)
          write(8,32)Ebarx
          WRITE(8,33)Nubarxt
    write(8,34)Gbarxt
          WRITE(8,35)zetaPG
          WRITE(8,36)zetaTE
          WRITE(8,37)zetaDELT
          WRITE(8,38)zetaPi
```

```
            WRITE(8,39)alphabarx
            WRITE(8,40)alphabarr

 32   format(' ','Ex=',e13.6)
 33   format(' ','Nuxt=',e13.6)
 34   format(' ','Gxt=',e13.6)
 35   format(' ','zeta PG =',e13.6)
 36   format(' ','zeta TE =',e13.6)
 37   format(' ','zeta DELT=',e13.6)
 38   format(' ','zeta Pi =',e13.6)
 39   format(' ','alpha x =',e13.6)
 40   format(' ','alpha r =',e13.6)
    RETURN
            END
!-------------------------------------------------------------------------------
!
!    Write Output
!
!
    SUBROUTINE Output
            Use var
            Use Plib
            implicit none
!
!     Echo Input
!
            write(8,*)title
            write(8,2)
            WRITE(8,*)'Laminate Stacking Sequence'
            WRITE(8,*)
            WRITE(8,32)
            DO k=1,nl
             write(8,33)lam(k)%mat_type,lam(k)%thick,lam(k)%theta
    end do
            write(8,2)
            write(8,*)'NRANK= ',nrank
            WRITE(8,36)Ri
    write(8,1)
            Do i=1,nm
     write(8,6)mat(i)%description
     write(8,7)mat(i)%e1, mat(i)%e2,  mat(i)%g12, mat(i)%pr12, mat(i)%pr23
             write(8,17)mat(i)%alpha1, mat(i)%alpha2
             write(8,1)
    end do
    Write(8,2)
    If(Pflag.eq.1)then
     Write(8,22)Px
    else
     Write(8,21)epsx
    end if
            If(Tflag.eq.1)then
```

```
      Write(8,24)T
     else
      Write(8,23)gammaxt
     end if
              write(8,25)Pin
              Write(8,26)Pout
              Write(8,27)deltaT
              write(8,2)
!
!
!
              Do i=1,nm
      Write(8,2)
              Write(8,*)'3D Stiffness Matrix C'
              Write(8,1)
              write(8,16)C(i,1),C(i,2),C(i,3),0.d0,0.d0,0.d0
              write(8,16)C(i,2),C(i,4),C(i,5),0.d0,0.d0,0.d0
              write(8,16)C(i,3),C(i,5),C(i,6),0.d0,0.d0,0.d0
              write(8,16)0.d0,0.d0,0.d0,C(i,7),0.d0,0.d0
              write(8,16)0.d0,0.d0,0.d0,0.d0,C(i,8),0.d0
              write(8,16)0.d0,0.d0,0.d0,0.d0,0.d0,C(i,9)
              Write(8,2)
     END DO
!
!
!
              DO k=1,nl
      Write(8,*)'Layer #',k
      Write(8,*)'C Bar Matrix'
      do i=1,6
       write(8,3)(CB(k,i,j),j=1,6)
      end do
              write(8,1)
              Write(8,*)'Off-axis CTE'
              do j=1,6
               Write(8,19)j,alpha(k,j)
      end do
              write(8,2)
     END DO
!
!
!
     Write(8,*)'Lamina Constants'
              WRITE(8,*)
              WRITE(8,34)
     Do k=1,nl
      WRITE(8,35)k,Lamda(k),Gamma(k),Omega(k),Sigmahat(k),Psi(k)
     END Do
              WRITE(8,2)
!
!
```

```
!
            Write(8,*)'Km Matrix'
!     Do i=1,10
!      Write(8,13)(KM(i,j),j=1,10)
!     end do
     Write(8,2)
     Write(8,*)'Rho & Elf Terms'
             write(8,15)
             Do i=1,2*nl+2
              Write(8,14)i,Rho(i),Elf(i)
     end do
             write(8,2)
!
!
!

            write(8,4)
            If(Pflag.eq.1)then
     Write(8,21)x(2*nl+1)
    else
             Write(8,22)x(2*nl+1)
    end if
            If(Tflag.eq.1)then
     Write(8,23)x(2*nl+2)
    else
     Write(8,24)x(2*nl+2)
    end if
            Write(8,2)
            write(8,*)'w(Ri)=',wri
!
!
!
             WRITE(8,2)
             WRITE(8,28)
             DO k=1,nl
              WRITE(8,29)k,r(k-1),epsr(k,1),epst(k,1),gamxt(k,1)
              WRITE(8,29)k,r(k),epsr(k,2),epst(k,2),gamxt(k,2)
     END DO
!
!
!
             WRITE(8,2)
             WRITE(8,30)
             DO k=1,nl
              WRITE(8,31)k,r(k-1),sigx(k,1),sigt(k,1),sigr(k,1),tauxt(k,1)
     WRITE(8,31)k,r(k),sigx(k,2),sigt(k,2),sigr(k,2),tauxt(k,2)
     END DO
!
!
!
 1    format(' ',/)
```

```
2   format(' ',//)
3   format(' ',6(2x,e9.2))
4   format(' ',5X,'SOLUTION')
5   format(' ','A1= ',d13.6)
6   format(' ','Material',3x,a32)
7   format(' ','E1=',en11.2,8x,'E2=',en9.2,10x,'G12=',en11.2,8x,'PR12=',f6.4,4x,'PR23=',f6.4)
8   format(' ','Lamda=',2x,En11.2)
9   format(' ','Gamma=',En11.2)
10  format(' ','Omega=',2x,En11.2)
11  format(' ','Sigmahat=',2x,En11.2)
12  format(' ','Psi=',2x,En11.2)
13  format(' ','|',10(2x,e11.4),1x,'|')
14  format(' ',2x,i2,4x,e11.4,4x,e11.4)
15  format(' ','Index',9x,'R',13x,'Elf')
16  format(' ','|',6(2x,e11.4),2x,'|')
17  format(' ','alpha1= ',en11.2,4x,'alpha2= ',en11.2)
18  format(' ','THETA= ',f8.4)
19  format(' ',i1,2x,en13.2)
20  format(' ','A2= ',e13.6)
21  format(' ','epsx= ',en15.6)
22  format(' ','Px= ',e13.6)
23  format(' ','gammaxt=',en15.6)
24  format(' ','T=',en13.6)
25  format(' ','Pin=',en13.6)
26  format(' ','Pout=',en13.6)
27  format(' ','delta T=',en13.6)
28  format(' ','Lamina',9x,'r',10x,'epsilon r',6x,'epsilon t',6x,'gamma xt')
29  format(' ',2x,i2,4x,e13.6,2x,e13.6,2x,e13.6,2x,e13.6)
30  format(' ','Lamina',9x,'r',11x,'sigma x',8x,'sigma t',8x,'sigma r',8x,'tau xt')
31  format(' ',2x,i2,4x,e13.6,2x,e13.6,2x,e13.6,2x,e13.6,2x,e13.6)
32  format(' ','Material Type',2x,'Lamina Thickness',2x,'Lamina Angle')
33  format(' ', 5x,i2,9x,en13.6,4x,f8.4)
34  format(' ','Lamina',6x,'lamda',10x,'Gamma',10x,'Omega',9x,'Sigmahat',9x,'Psi')
35  format(' ',2x,i2,2x,5(2x,e13.6))
36  format(' ','Ri= ',en15.6)
    RETURN
    END
```